

AD-A227 606

**RFQ Lens for LEBT Applications**  
**Final Report**

Principal Investigator: D. A. Swenson  
(619) 458-3854

Submitted to:

**USASDC**  
Under Contract DASG60-89-C-0084

Period of Performance: June 13, 1989 to June 30, 1990

August 31, 1990

**BEST  
AVAILABLE COPY**

DISTRIBUTION STATEMENT A
Approved for public release;
Distribution Unlimited

DTIC  
ELECTE  
SEP 17 1990  
S E D

## TABLE OF CONTENTS

SECTION	PAGE
1 SUMMARY.....	1
2 RFQ LENS BACKGROUND.....	4
3 PROPERTIES OF RFQ LENSES .....	5
4 PERFORMANCE OF RFQ LENSES .....	12
5 ELECTRICAL ENGINEERING ANALYSIS OF RFQ LENSES.....	22
6 DESIGN OF RFQ LENS FOR PROOF-OF-PRINCIPLE EXPERIMENT .....	23
7 PRE-BEAM TESTS AND FINAL VANE DESIGN FOR THE RFQ LENS SYSTEM.....	41
8 BEAM TESTS AT FERMI NATIONAL ACCELERATOR LABORATORY.....	46
9 POST BEAM TEST OBSERVATIONS.....	56



A-1

STATEMENT "A" per Brandt Garner  
US Army Strategic Defense Command/CSSD-DE  
N, PO Box 1500, Huntsville, AL 35807-3801  
TELECON 9/17/90 VG

## 1. SUMMARY

Through a Broad Agency Announcement (BAA DASG60-87-176), the U. S. Army Strategic Defense Command (USASDC) solicited proposals for new and innovative particle beam technologies which are relevant to the Neutral Particle Beam (NPB) Program. Since high brightness beams are required for NPB and beam emittance, in large part, is determined by the ion source and low energy matching section, innovations to improve the quality or efficiency of the low energy beam transport (LEBT) are important. Some preliminary studies on radio frequency quadrupole (RFQ) lenses indicated that such lenses could be developed with improved capabilities for preparing ion beams for injection into RFQ linacs. These improved capabilities derive from the fact that the focusing effect is inversely proportional to the square of the frequency so stronger focusing can be achieved if the frequency in the RFQ lens is less than that of the RFQ linac. The goal of this project is to design, build, and test an RFQ lens that demonstrates the possibility of decoupling the phase and frequency of the RFQ lens from that of the RFQ linac into which it is focusing ions. SAIC was awarded Contract No. DASG60-89-0084 on June 13, 1989 with a contract duration of 6 months for this purpose.

The design of the lens was based on two-dimensional beam dynamics and RF cavity geometry analyses performed with the TRACE and SUPERFISH codes, respectively. The lens was then fabricated by a combination of SAIC and subcontracted machine shops. After fabrication, the lens was assembled for verification of resonant frequency, mode separation, tuning, and power conditioning, prior to beam tests, at Fermi National Accelerator Laboratory (FNAL). In the course of these measurements, it was determined that the resonant frequency was much higher than predicted by the two-dimensional analysis (the measured value was 588 MHz compared to the predicted value of 300 MHz). Since the rf focusing effect is larger for lower frequencies — a key feature of the RFQ lens — this discrepancy had to be understood. Therefore, although not planned or budgeted for this project, three-dimensional ARGUS calculations were performed which confirmed the measurements. These calculations indicated that three-dimensional end effects were the cause of the elevated frequency. This conclusion was also confirmed by network analyzer measurements on a mocked-up geometry.

Two possible responses to this observation were feasible: one was to fabricate a new, larger diameter lens, and the other was to modify the geometry of the vanes in the existing lens to load the cavity and thereby reduce the resonant frequency. In the interests of budget and schedule, the latter option was chosen. By changing the geometry of the vanes, the inductance and capacitance of the lens were changed and a resonant frequency of 300 MHz was achieved. However, these

modifications also caused the  $Q$ , a measure of power-coupling efficiency of the cavity, to decrease by a factor of approximately five. The modified lens is shown in Fig. 1.



Fig. 1. RFQ Lens with One Cover Plate Removed.

Following a successful full power (26 kW) test of the close-coupled rf (CCRF) power system at SAIC, the lens and CCRF system were shipped to FNAL for experiments on a duoplasmatron ion source test bench which generates a 20-keV proton beam. The objective of the test was to measure whether beam focusing occurred and if the focusing effect varied with rf power as expected. While focusing and tuning were observed, the performance was not as expected nor is it completely understood. The inconclusive nature of the results can be related to two important

conditions which prevailed during the experiment. The first is that the rf used to power the lens interfered strongly with the emittance scanner, making even rough emittance measurements difficult at best. The second is that, due to the reduced Q of the lens and the limit of 26 kW of available rf power, the lens was underpowered by a substantial factor. With these conditions, the proton focusing effect would have been too small to be observed by the emittance scanner operating with rf interference. This conclusion was born out by subsequent TRACE calculations.

However, on the last day of the five-day experiment, after working to minimize rf interference with the emittance scanner and maximizing rf power, a round spot was seen on a viewing screen. The radius of the spot varied with lens excitation as expected. Although TRACE calculations indicate that the lens excitation was inadequate to focus the 20 keV proton beam, we speculate that these observations indicate the focusing of some undefined component of the beam. Further TRACE calculations to identify this component have failed to shed further light on the phenomenon.

Sections 2-5 describe some of the general results obtained in the course of defining the lens design. The remaining sections describe the specifics of the design, fabrication, testing, and conclusions drawn from the proof-of-principle device.

Whether this RFQ lens successfully demonstrated focusing is open to interpretation. However, no results were obtained that would suggest any problem with the basic concept. Furthermore, much was learned in this project to suggest substantial improvements that could be made to the lens design. Considering its potential advantages for NPB, we believe the RFQ lens is worthy of further study by the USASDC.

## 2. RFQ LENS BACKGROUND

The advent of the RFQ linac has produced the need for a means of focusing low energy (10-50 keV) particle beams in the low energy beam transport (LEBT) section of the accelerator. Achieving the required strongly convergent beam with quadrupole magnets or solenoid lenses has become a problem. The lower beam energies give added impetus to the use of electric, as opposed to magnetic lenses, in these regions.

The RFQ lens is an electric quadrupole lens with the added advantages that no insulators are required to support the resonant electric fields in the structure and the required "alternating gradient" feature is provided by the temporal alternation in the polarity of the fields.

RFQ lenses are inherently simpler than RFQ linacs. They have been around longer than their linac counterpart, finding application in atomic physics, plasma physics, and mass spectroscopy. Prior to this initiative, however, they were thought to be too weak in focusing strength to serve the demanding application of matching low-energy ion beams into modern RFQ linacs.

A key observation, which motivated this project, is that there are some configurations of RFQ lenses whose effect on the beam is independent of the phase of the rf excitation at the time that the particle enters the lens. This, in turn, suggests that these configurations do not have to be synchronized with the linac phase or frequency to have a useful focusing effect on the beam. This observation has been validated by TRACE particle dynamics calculations which will be described later in this report. In particular, it suggests that RFQ lenses could be designed to operate at a lower frequency than the linac where their strength would be substantially stronger.

### 3. PROPERTIES OF RFQ LENSES

The focusing strength for RFQ devices is proportional to  $B = E\lambda^2/(r(m/q))$ , where  $E$  is the surface electric field on the tip of the electrode,  $\lambda$  is the rf wavelength,  $r$  is the radial aperture of the electrodes, and  $m/q$  is the mass-to-charge ratio of the beam particles. If  $E$  is expressed in units of MV/m,  $\lambda$  in meters,  $r$  in meters,  $m$  in MeV, and  $q$  in multiples of the proton charge, the quantity  $B$ , which we will call the "B-value" or focusing strength of the RFQ, is unitless. For example, for the lens which was built for this project,  $E=11.2$  MV/m,  $r=0.01$  m,  $\lambda=1.0$  m,  $q=1$ , and  $m=938$  MeV, leading to a B-value of 1.2.

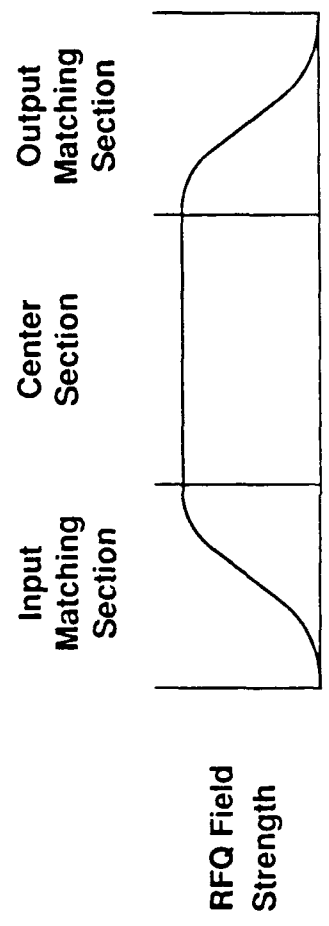
The optimization of RFQ linacs for focusing and acceleration of small diameter particle beams essentially precluded the use of RFQ lenses, operating at the linac frequency, on the larger diameter beams in LEBTs, because of inadequate lens strength. The key observation, presented here, is that there are some configurations of RFQ lenses that do not have to be at the linac frequency in order to effect a useful transformation on the beam and, in particular, may operate at a lower frequency where their strengths can be substantially higher.

The basic components and performance of an RFQ lens for LEBT applications are shown in Fig. 2. The lens comprises three sections, namely, the input matching section, the center section, and the output matching section. It is the proper configuration of the two matching sections that gives the all-important phase independence of the focusing action. The RFQ field strength in the two matching sections must increase smoothly from zero to full strength over some minimum distance, or vice versa, to allow the beam to adapt to the time-varying rf fields within the lens.

The beam profiles through the basic RFQ lens, as displayed by the TRACE program, are shown in the lower part of Fig. 2. The horizontal profiles are shown above the center line and the vertical profiles are shown below. The four different trajectories, seen in each profile near the center of the lens, correspond to four different phasings of the beam relative to the lens excitation.

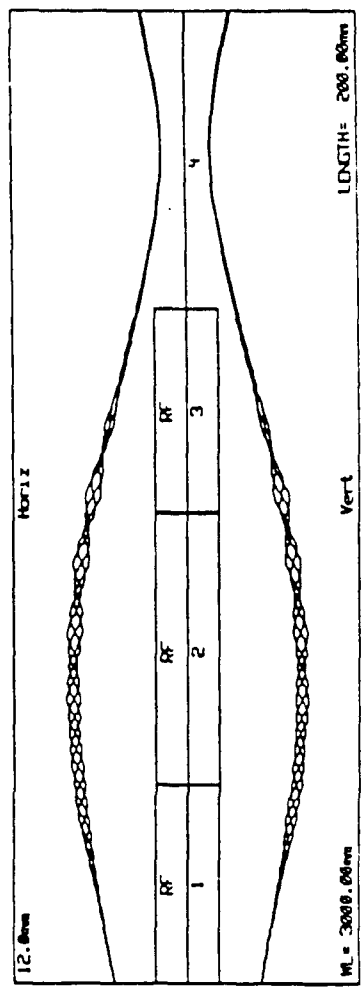
Figure 3 shows the transverse phase spaces (the six boxes at the top of the figure) and the beam profiles (the large box at the bottom of the figure) for four beams, separated by  $90^\circ$  in phase, at the beginning (left), middle, and end of an RFQ lens. The phase spaces display the transverse dimensions of the beam versus the angular divergence of the beam. The beams are considered to occupy the elliptical regions in the transverse phase spaces. The A and B values in each box correspond to the  $\alpha$  and  $\beta$  twiss parameters respectively for the four beams.

# Three Components of RFQ Lens.



RFQ Field Strength

## X Profile



## Beam Profiles:

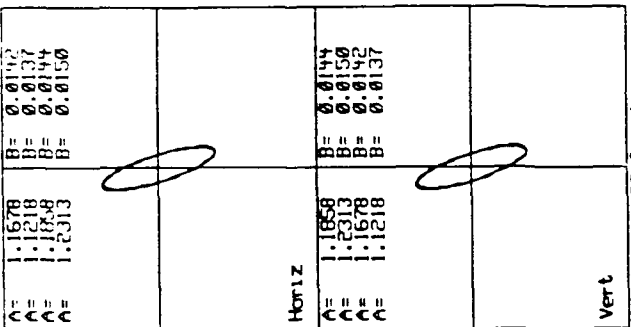
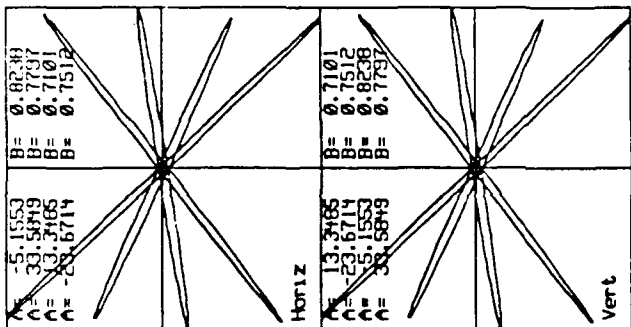
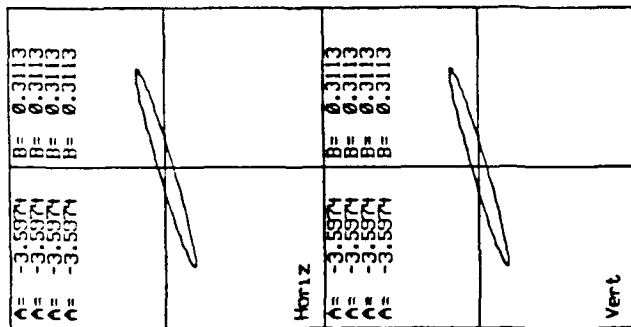
Large divergent beam into RFQ Lens

## Y Profile

Fig. 2. Basic Components and Performance of an RFQ Lens.



Four Beams  
Separated by  
90° in Phase.



Output is  
Phase  
Independent !

Beam Profiles:  
Large divergent beam  
into RFQ Lens

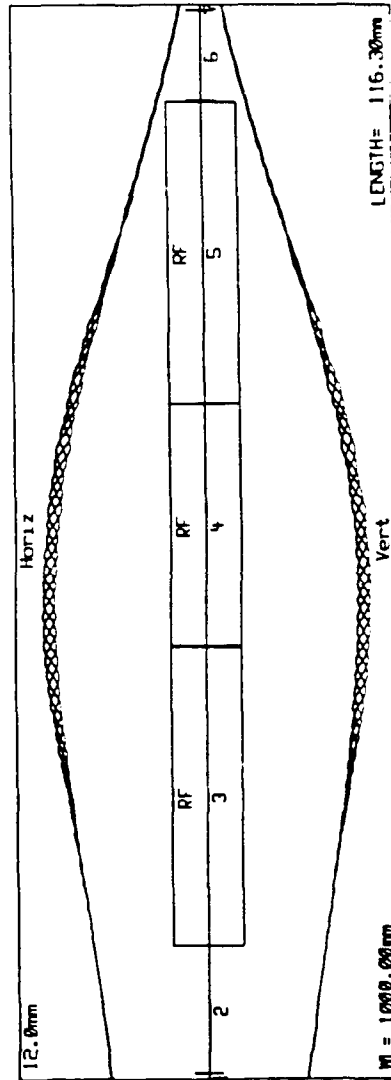


Fig. 3. Phase Space at the Beginning, Middle, and End of RFQ Lens.

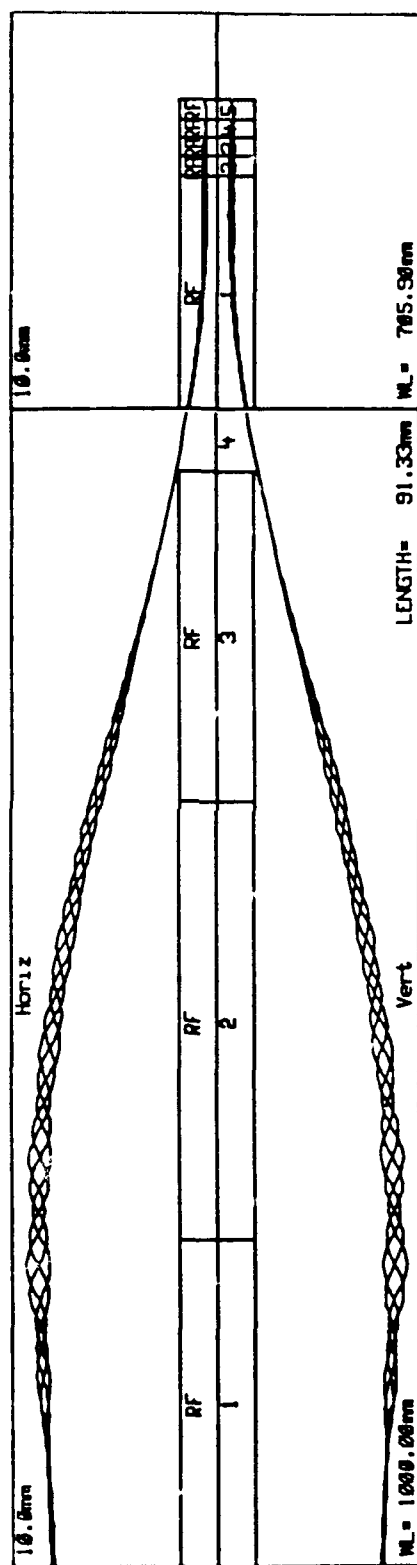
The phase space and profiles of the four beams are chosen to be identical at the input side of the figure. In the middle of the lens, the phase spaces occupied by the four beams are dramatically different. The fact that these phase spaces and profiles coalesce at the end of the lens demonstrates that the lens action is independent of phase.

Consider a beam in a LEBT that is ten times the diameter of the beam in a 425-MHz RFQ linac. Because the radial aperture of the lens electrode must be ten times larger than that of the linac in order to accommodate the beam, the achievable RFQ lens strength in the LEBT at the frequency of the RFQ linac is down a factor of ten from that in the linac. Since the focusing strength is proportional to the square of the rf wavelength, the possibility of using a 100-MHz lens, instead of a 425-MHz lens, regains that order of magnitude in strength.

Figure 4 shows an example of an RFQ lens focusing a relatively large-diameter, high-current (65 mA) beam into a strongly convergent beam for injection into a modern RFQ linac (the beam moves from left to right in the figure). Most alternative lens systems require that beams of this current be neutralized to reduce the space charge defocusing of the beam. The possibility of matching high-current beams into modern RFQ linacs, without the extra complication of beam neutralization, suggests a unique capability for the RFQ lens.

Another unique feature of the RFQ lens is its ability to achieve short focal lengths for large diameter beams, utilizing quadrupole focusing, while maintaining nearly circular cross-sections for the beams. This requires focal periodicities that are short relative to the diameter of the beam. Figure 5 illustrates why this is impractical for electrostatic or magnetostatic quadrupole lens systems and practical for the RFQ lens. In the static cases, the field limitations are longitudinal and the field pattern is highly three dimensional. In the rf case, the field limitations are transverse and the field patterns are primarily two dimensional, which may in turn reduce beam aberrations. In addition, the transverse field limitations are much higher than the longitudinal limits, which leads to higher focusing strength and shorter focal lengths.

A wide variety of match conditions are possible with the RFQ lens. The output of the RFQ lens has azimuthal symmetry as required by the input to RFQ linacs. Consequently, matching a beam to an RFQ linac with an RFQ lens may require only two adjustable parameters compared to the four adjustable parameters required by the static quadrupole system. The two adjustable parameters could be lens excitation and lens position. Another approach would be to have two RFQ lenses in tandem to provide the two adjustable parameters.



RFQ Lens  
300 MHz

RFQ Linac  
425 MHz

Fig. 4. Beam Profiles Through an RFQ Lens and into an RFQ Linac.

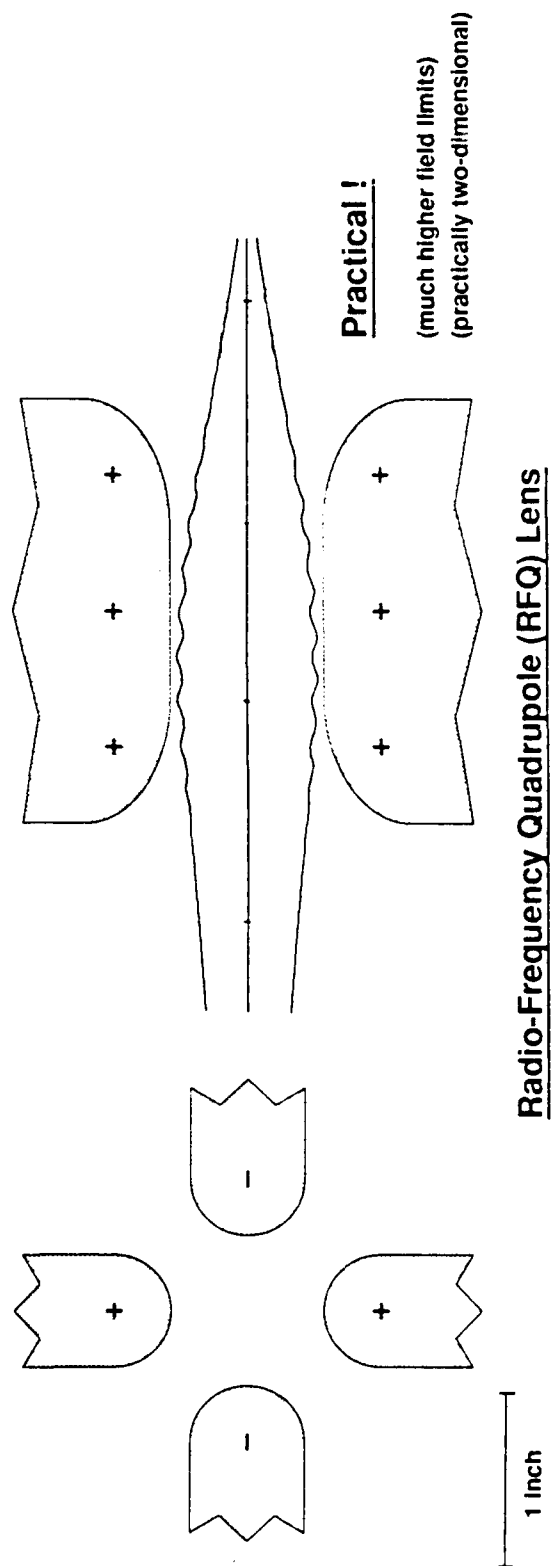
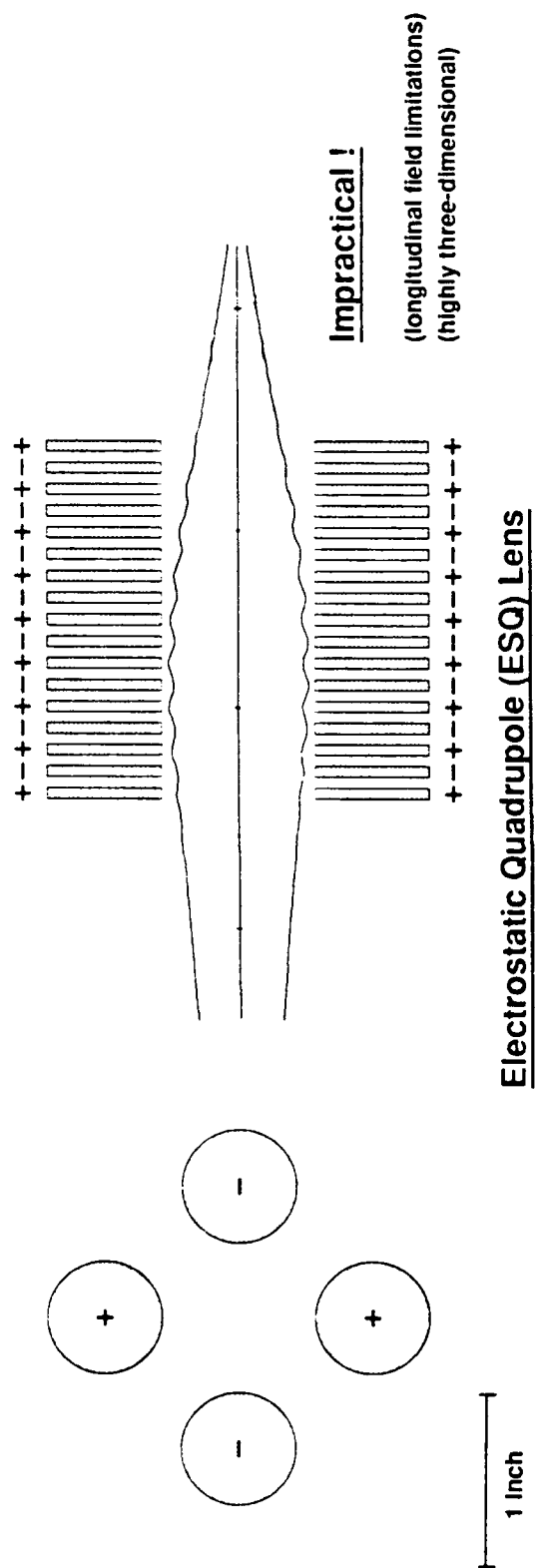


Fig. 5. Comparison of Static and RF Quadrupole Lens Systems.

In summary, the RFQ lens exhibits a net focusing in each transverse plane, maintains a near circular beam throughout the lens, may be exceptionally low in aberrations, has no frequency or phase constraint to subsequent linac structures, has acceptable surface field strengths, and is tunable, simultaneously in both transverse planes, by rf amplitude.

#### 4. PERFORMANCE OF RFQ LENSES

In this section, we illustrate some of the performance features of RFQ lenses. The interactive beam dynamics code, TRACE, was used to calculate beam profiles for different RFQ lens lengths, strengths and frequencies, and different beam particle masses, charges, energies, emittances and twiss parameters. These calculations were done in order to improve our understanding of the lens performance, guide the design of the proof-of-principle device, and explore different regions of operation without the expense of fabricating hardware.

A tapered (or non-tapered) RFQ section is described by five parameters in the TRACE code, namely, 1) the upstream focusing strength (B), 2) the downstream focusing strength, 3) the length of the element in units of the particle wavelength ( $\beta\lambda$ ), 4) the number of computational steps through the element, and 5) the rf phase at the entrance to the element (in degrees). A data file for a typical RFQ lens calculation is shown in Fig. 6. The input and output matching sections are prescribed by controlling the upstream and downstream focusing strengths. An "S-shaped", as opposed to linear, ramp is prescribed by setting the fourth parameter to be negative. This simple TRACE model of the lens involves 5 elements where the first and last elements are drift spaces and the middle three are the three sections of an RFQ lens. For this input, the particle rest mass (ER) correspond to that of an  $H^-$  ion and the particle energy (W) is .02 MeV (20 keV). The wavelength (WAVEL) of the rf excitation is 1500 mm corresponding to a frequency of 200 MHz. The beam current (XI) in this case is 16 mA. The TRACE calculation that results from this file data file is shown in Fig. 7.

Figures 8 to 12 describe some sets of TRACE calculations that illustrate the performance of RFQ lenses for different particle types (Figs. 8 and 9), different input emittances (Fig. 10), different beam currents (Fig. 11), and different lens excitations (Fig. 12). Figure 8 shows the beam profiles, in a specific RFQ lens, for four different particle beams:

- Proton beam,  $m=1$ ,  $q=1$ ,  $V(\text{inj}) = 10 \text{ kV}$ ,  $V(\text{rfq}) = 30 \text{ kV}$ ,
- Deuteron beam,  $m=2$ ,  $q=1$ ,  $V(\text{inj}) = 20 \text{ kV}$ ,  $V(\text{rfq}) = 60 \text{ kV}$ ,
- Helium-3 beam,  $m=3$ ,  $q=2$ ,  $V(\text{inj}) = 15 \text{ kV}$ ,  $V(\text{rfq}) = 45 \text{ kV}$ ,
- Helium-4 beam,  $m=4$ ,  $q=2$ ,  $V(\text{inj}) = 20 \text{ kV}$ ,  $V(\text{rfq}) = 60 \text{ kV}$ ,

where  $m$  and  $q$  are in units of the proton mass and charge.

```

'REMEMBER UNITS ARE mm AND mrad (QUAD=T/m)
'ER      W      Q      DP/P'
939.23000 0.02000 1.00000 0.00000
'XI      SMAX   EXI   EYI'
16.00000 2.00000 153.00000 153.00000
'BEAMI:alphaX betaX  alphaY  betaY'
-8.75610 0.20510 -9.26660 0.24170
'BEAMF:alphaX betaX  alphaY  betaY'
4.43000 0.04300 4.43000 0.04300
'WAVEL    XM     XPM     XYM'
1500.00000 10.00000 400.00000 25.00000
'MRG 1-4      IXW      IYW      IYP'
1000 4000 50 3050 900 900 1100
'N1  N2  NV  MT  PQEXT'
1    5    4    1    0.000

'ME  MP  CONV'
1    1    1.0000
2    1    1.0000
6    1    1.0000
7    1    1.0000

'COMMENTS  NE  NT  PARAMETERS'
1    1    24.49572  0.00000  0.00000  0.00000  0.00000
2    8    0.00000  2.00000  3.00000 -48.00000  0.00000
3    8    2.00000  2.00000  4.00000 64.00000  0.00000
4    8    2.00000  0.00000  3.00000 -48.00000  0.00000
5    1    23.84074  0.00000  0.00000  0.00000  0.00000

'PE  PP  PCONV'
0    1    1.0000
0    1    1.0000
0    1    1.0000
0    1    1.0000
0    1    1.0000
0    1    1.0000

```

Fig. 6. TRACE Data File for Typical RFQ Lens Calculation.

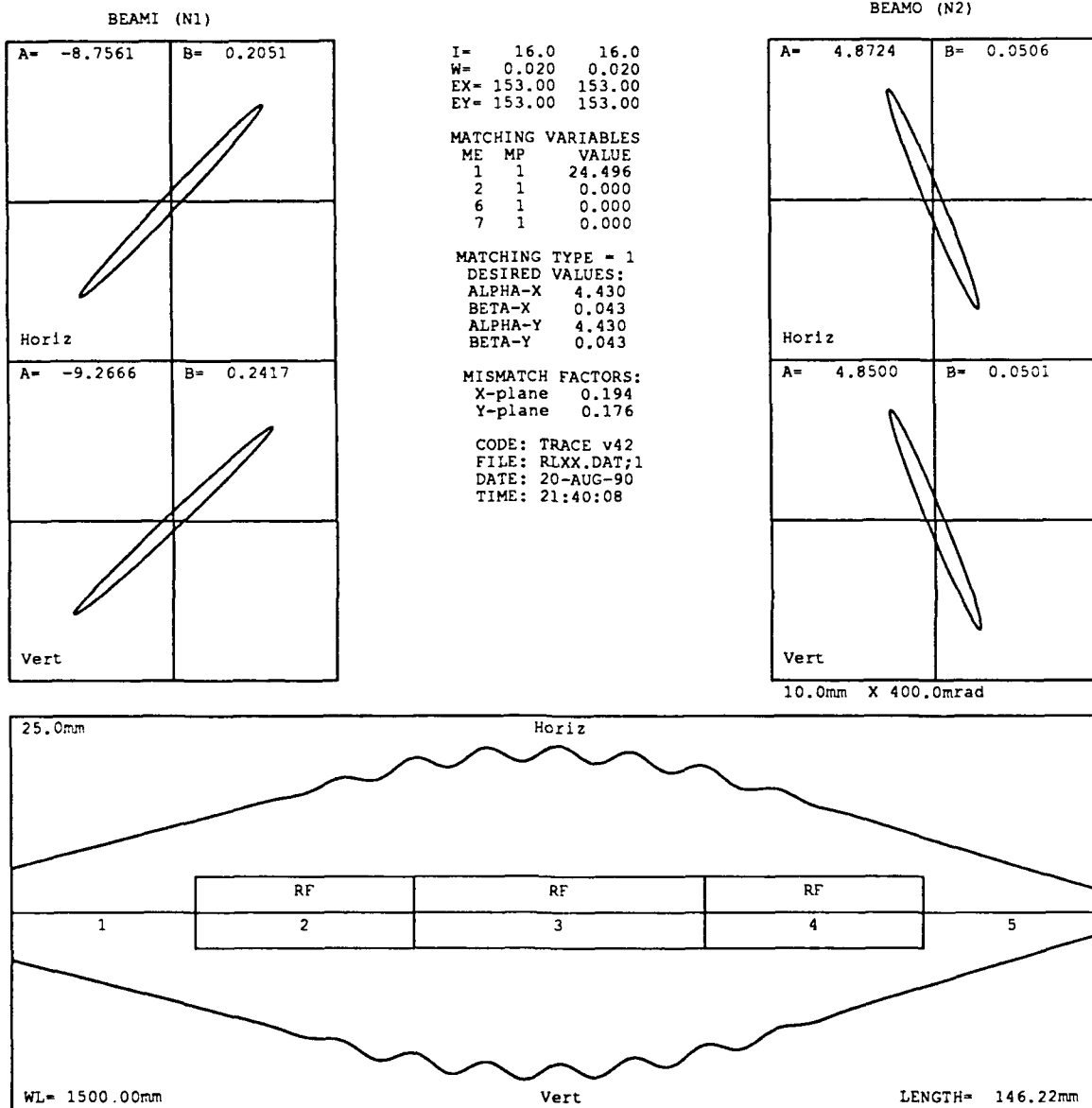


Fig. 7. Typical TRACE Output for RFQ Lens Calculation.



Particle	M	Q	V(inj)	V(rfq)
proton	1	1	10	30
deuteron	2	1	20	60
helium-3	3	2	15	45
helium-4	4	2	20	60

Similar Performance when  $V_s \approx M/Q$

Same constraint that all RFQ operate under.

Scaling Law:

$V(\text{inj})$  and  $V(\text{rfq}) \approx M/Q$

(Law of constant velocity)

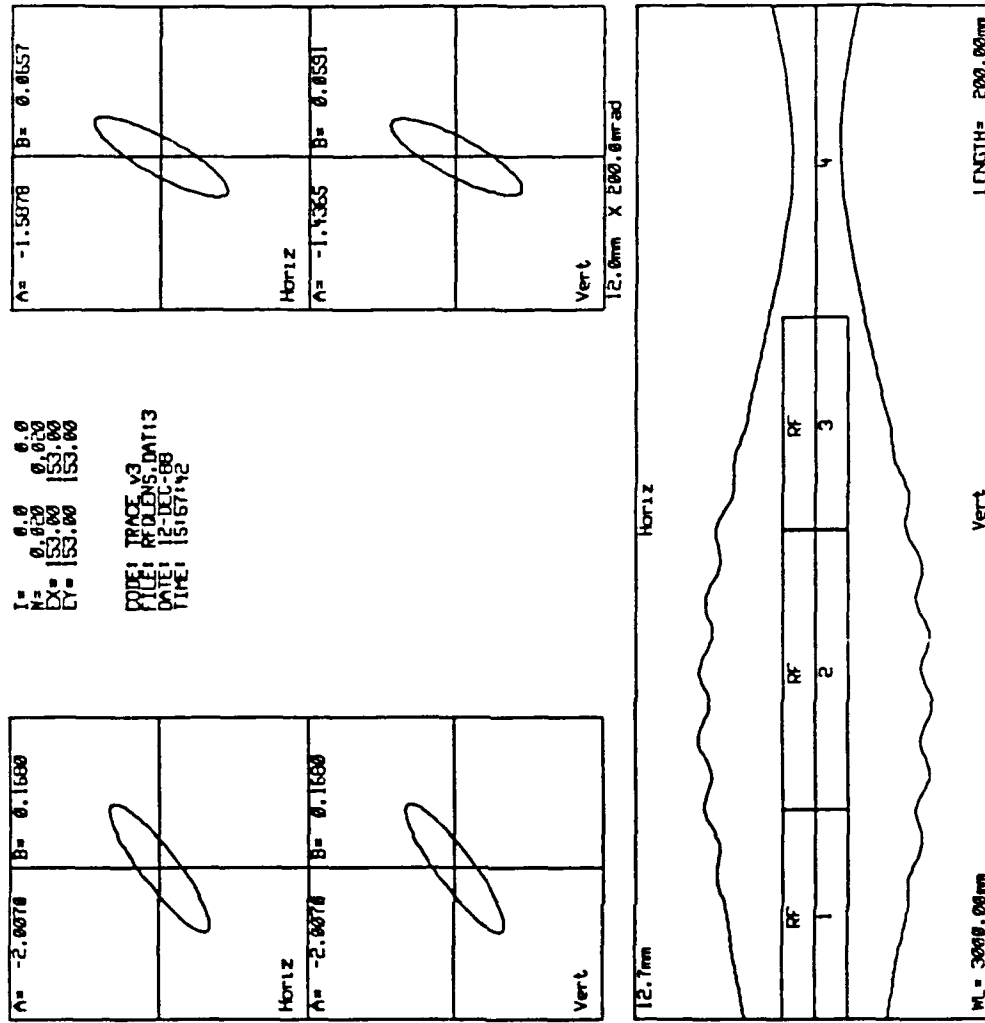
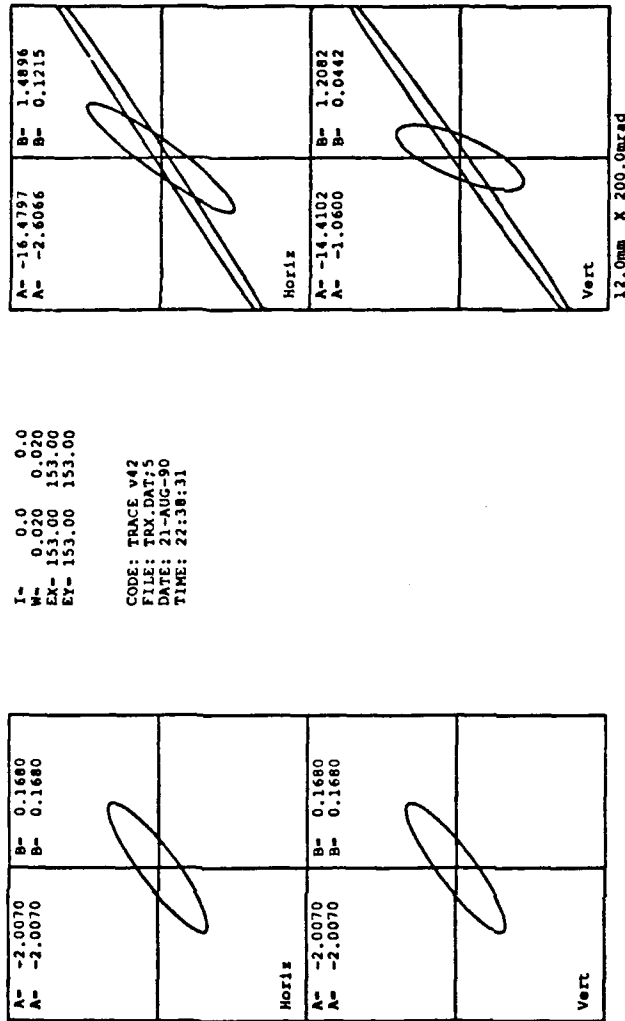


Fig. 8. Beam Profiles for Different Particle Beams.

**Over focussed beam:**

**Profile of a 20 keV proton beam  
in an RFQ lens designed to  
focus a 20 keV deuteron beam.**



**Focussed beam:**

**Same conditions with RFQ excitation  
decreased by a factor of 0.707.**

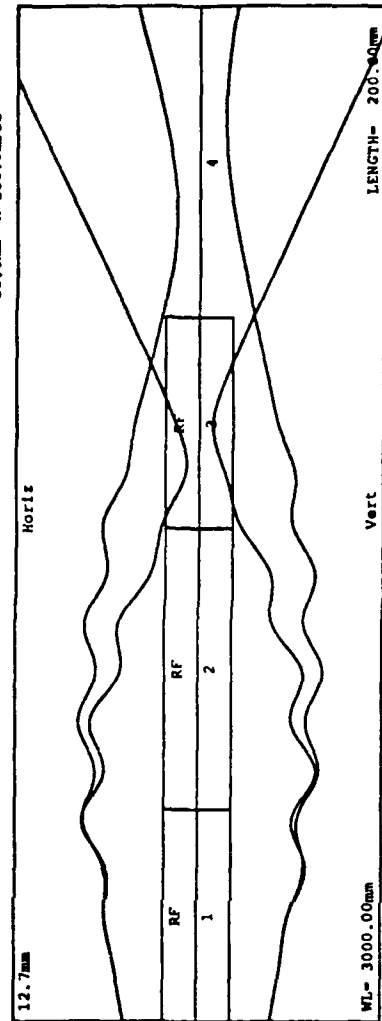


Fig. 9. Beam Profiles for 20-keV Proton and Deuteron Beams.

## Emittance Values

50 cm-mrad  
100 cm-mrad  
150 cm-mrad  
200 cm-mrad  
250 cm-mrad  
300 cm-mrad

Focal Properties are  
independent of the  
emittance of the beam.

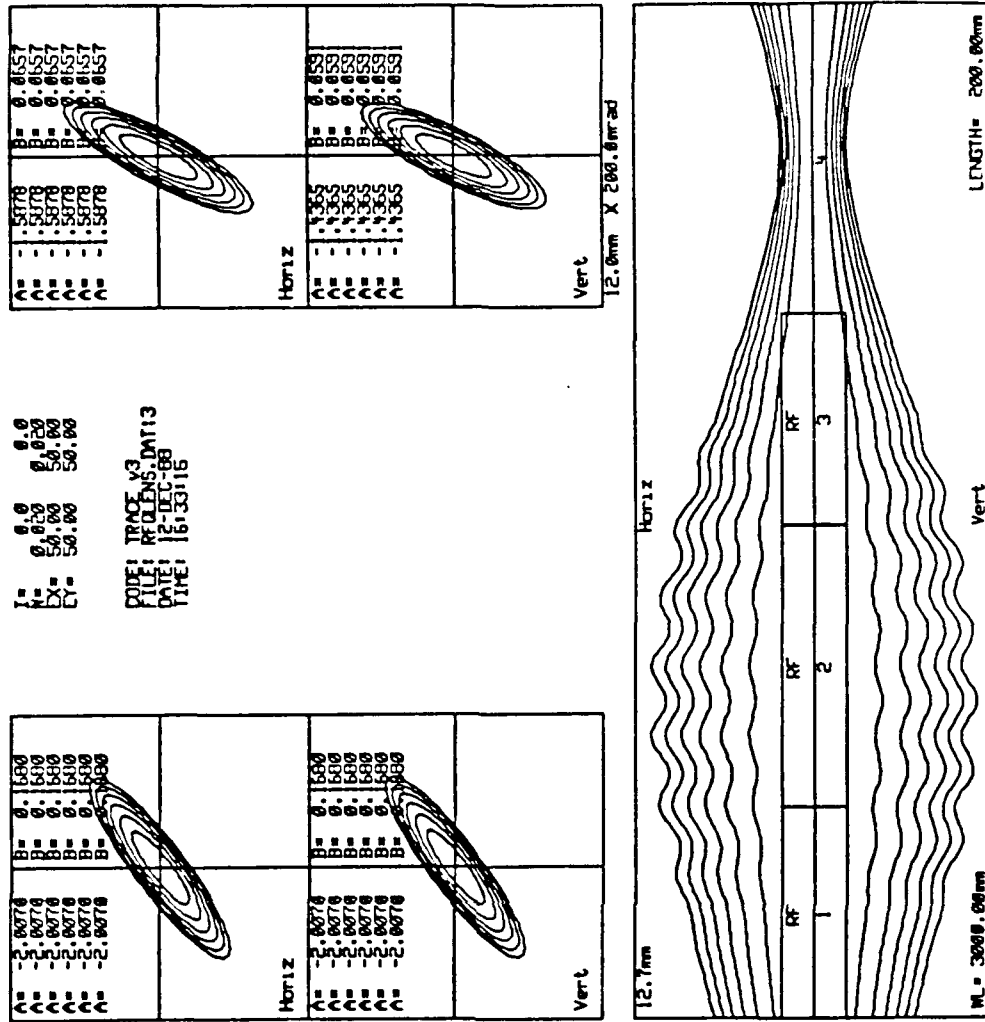


Fig. 10. Beam Profiles as a Function of Emittance.

# Beam Currents

0 mA  
10 mA  
20 mA  
30 mA

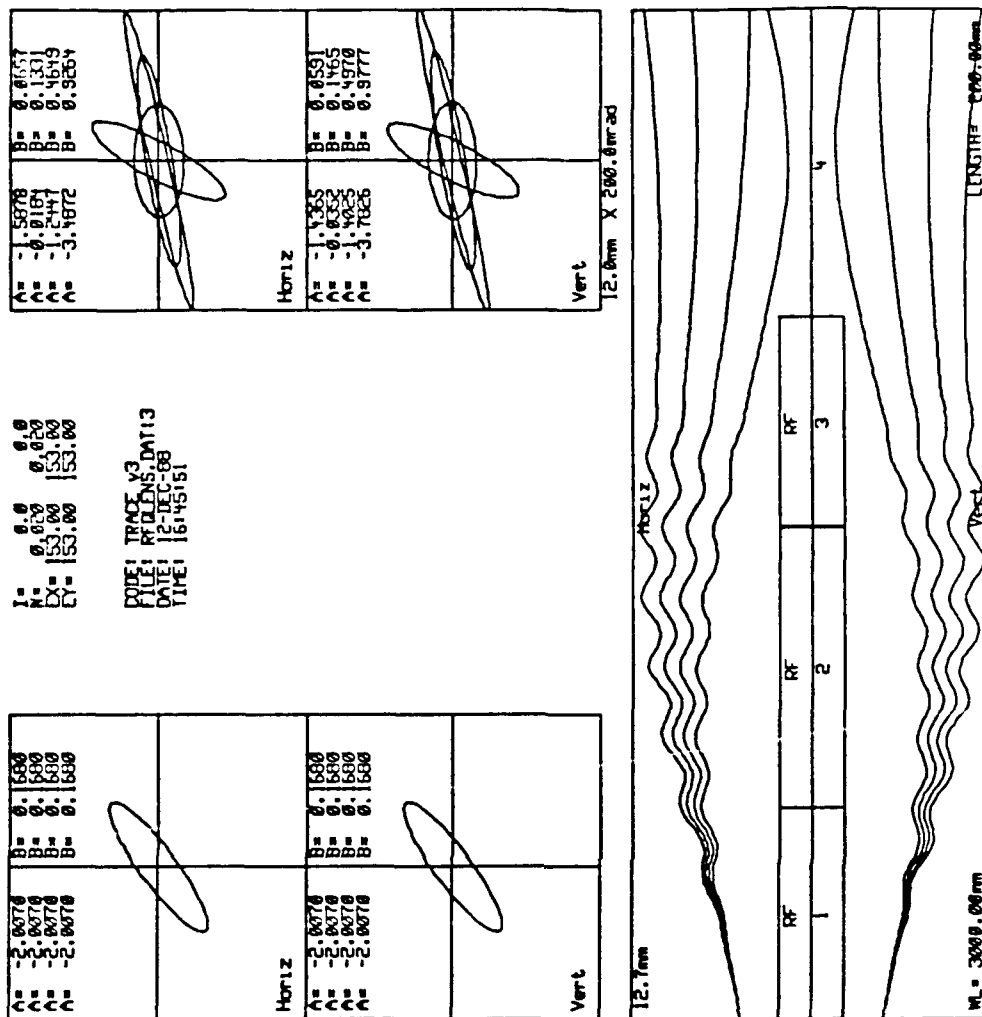


Fig. 11. Beam Profiles as a Function of Space Charge.

# B-Value

2.6  
2.8  
3.0

Changes in lens  
excitation can  
acomodate changes  
in space charge  
repulsion.

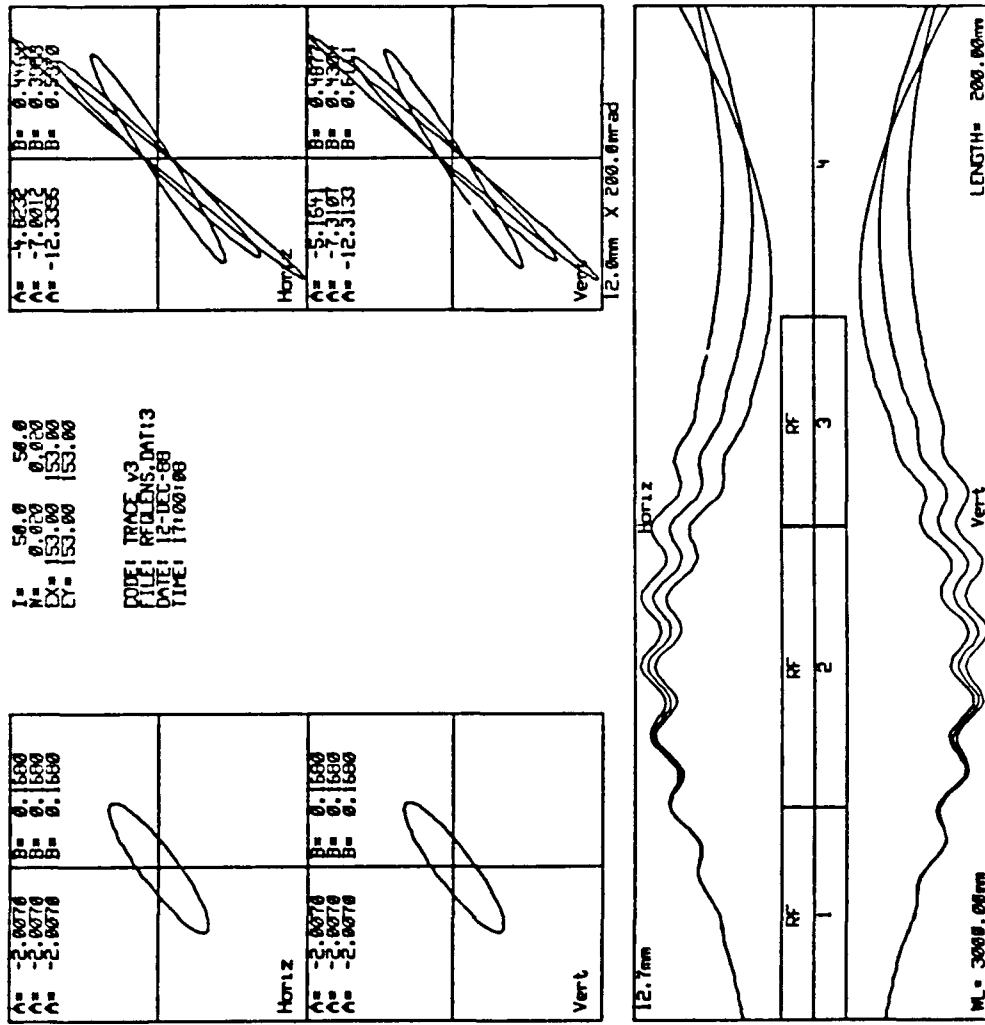


Fig. 12. Beam Profiles as a Function of RFQ Lens Strength.

Here, we see that the focal properties of a specific RFQ lens are independent of the mass and charge of the ion, provided the injection voltage and the lens excitation are varied directly with the  $m/q$  of the ion. This is the same constraint under which all RFQs operate, namely that the injection velocity must agree with the value for which the RFQ was designed.

Figure 9 shows the beam profile of a 20 keV proton beam in an RFQ lens designed for 20 keV deuterons. A decrease in  $V$  (RFQ) by a factor of 0.707 restores the profile close to the design profile.

Figure 10 shows the beam profiles of six deuteron beams, with TRACE emittance values of 50, 100, 150, 200, 250, and 300 mm-mrad, in an RFQ lens with the excitation of 60 kV. Hence, we see that the focal properties of a specific RFQ lens are independent of the emittance of the beam.

Figure 11 shows the beam profiles of four beams of current 0, 10, 20, and 30 mA in a channel designed for zero current. Hence, we see the effect of beam current on beam profile. Space charge effects can be countered by adjusting lens excitation, as shown in the figure.

Figure 12 shows the beam profiles of a 50 mA deuteron beam with RFQ B-values of 2.6, 2.8, and 3.0. Hence, we see that changes in lens excitation can accommodate for space charge repulsion.

The RFQ lens, like the more familiar magnetic quadrupole lens, can be applied to a very wide range of particle beam types, currents, energies, and emittances. The RFQ lens, being electric in nature, has important strength advantages over magnetic lenses at the low particle velocities found in most present-day LEBTs.

The RFQ lens differs from an electrostatic quadrupole lens because of the time-dependent nature of its electric fields. Unlike an electrostatic lens, it can discriminate between different ion species in a particle beam. The RFQ lens is similar to a magnetic lens in that it focuses lighter particles more strongly than heavier particles of the same charge and energy.

The choice of the optimum length and frequency for a specific application of the RFQ lens is complicated by the interplay between two competing phenomenon. We have seen that the strength of a lens can be increased by reducing the rf frequency. The strength can also be increased by making the lens longer, giving the electric fields longer to act on the particles. Longer and lower frequency lenses are thus stronger, allowing a reduction in the electric field gradient and a savings in rf power.

However, for systems involving highly divergent or convergent beams, the longer and/or lower frequency systems usually result in larger beam excursions. Longer lenses require less electric field gradient, which implies lower surface electric fields and less rf power. Larger-aperture lenses require the same electric field gradient as smaller-aperture lenses, which implies that the larger-aperture lenses must use higher surface electric fields and more rf power. In some cases, longer lenses, with their lower electric field gradients, will allow larger beam excursions, which, in turn, will require larger lens apertures and more rf power. This puts an upper bound on the lens length for some lens applications.

Lowering the lens frequency carries with it a concomitant lengthening of the lens due to the fact that in the input and output radial matching sections, the electric field gradient must increase smoothly from zero to full strength, or vice versa, to allow the beam to adapt to the time-varying rf fields within the lens. Design experience suggests that these sections should each be about three particle wavelengths in length; shorter sections result in significant beam emittance growth. In some cases, lower frequencies, with longer matching sections, will result in lenses that allow larger beam excursions, which, in turn, will require larger lens apertures and more rf power. This puts a lower bound on the frequency for some lens applications.

## 5. ELECTRICAL ENGINEERING ANALYSIS OF RFQ LENSES

The particle dynamics analysis of the previous section guides the designer in the specification of lens properties required to achieve the desired focusing effect on the particle beam. Further work must then be done to transform these properties an engineering design. For example, TRACE calculations may indicate that a B-value (focusing strength) of 1.2 is adequate for the application at hand. This must be transformed into a design having a specific frequency and electrode aperture. Other engineering data required for the design include the dimensions and shape of the cavity, rf power losses on the cavity surfaces, the distribution of electric fields within the cavity, and the total stored energy in the cavity fields. It is particularly important to complete such calculations when designing an RFQ lens which involves new applications, new frequencies, new geometries, and/or new fabrication techniques.

We have used the two-dimensional computer code SUPERFISH for these analyses. SUPERFISH is a popular choice to provide the required engineering data for RFQ linacs, drift tube linacs, coupled-cavity linacs, and rf power sources. SUPERFISH is restricted to the evaluation of axisymmetric cavity modes in axisymmetric rf cavities. Nevertheless, SUPERFISH results are very informative and generally provide most of the data required by designers.

For example, SUPERFISH is used to analyze RFQ linacs by taking the two-dimensional cross section of the linear structure as the cross-section of a large torus, thus converting it into an axisymmetric geometry. A special postprocessor for the output (SFO5) translates the results for the toroidal geometry back into a format that is more relevant to a linear geometry. This format includes the resonant frequency, the maximum surface electric field, the maximum surface magnetic field, the power dissipation/meter, the stored energy/meter, the quality factor (Q), the average RFQ gradient, the RFQ aperture, the vane-to-vane voltage, and the shunt impedance of the structure. In conventional RFQ linacs, which are long compared to their diameter, the geometry of the cavity terminations (end effects) have little effect on the resonant frequency or electrical properties of the structure. In these cases, the important properties of the cavity are determined primarily by the transverse dimensions of the cavity, where the two-dimensional SUPERFISH calculations suffice. SUPERFISH results for the RFQ lens which was constructed for this project will be displayed and discussed in subsequent sections which deal with this specific design.

It should be noted here, however, that in some cases three-dimensional calculations, with their attendant costs and complexities, are required to understand fully and engineer some aspects of RFQ cavities. Vane tip modulations and end effects are examples of such features. Suitable computer codes for these calculations are MAFIA (a German code) and ARGUS (an SAIC code).



## 6. DESIGN OF RFQ LENS FOR PROOF-OF-PRINCIPLE EXPERIMENT

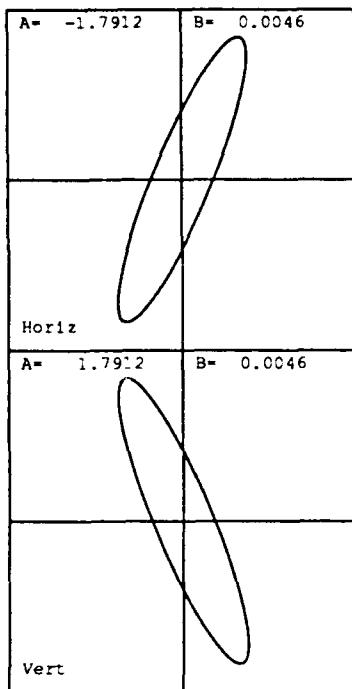
The most immediate and demanding application for the RFQ lens is to focus low-energy ions into RFQ linacs. The design goal for this project was to demonstrate an RFQ lens which could focus a slightly divergent, 20-mA beam of 20-keV protons into a modern 425-MHz RFQ linac structure. For design purposes, the emittance and twiss parameters for the 20-keV proton beam at the entrance of the lens were taken to be as follows:

$$\begin{aligned}\epsilon_{n,rms} &= 0.020 \text{ cm-mrad} \\ \beta\lambda &= 0.00653 \\ \epsilon_{u,trace} &= 122 \text{ mm-mrad} \\ \alpha_{twiss} &= -2.4 \\ \beta_{twiss} &= 1.2 \text{ mm/mrad}\end{aligned}$$

where  $\epsilon_{n,rms}$  refers to the normalized, rms emittance;  $\epsilon_{u,trace}$  refers to the unnormalized, 90% emittance envelope used in TRACE;  $\alpha_{twiss}$  and  $\beta_{twiss}$  are the usual Twiss beam parameters;  $\beta$  is the velocity of the particle divided by the speed of light; and  $\lambda$  is the Compton wavelength of the particle. These parameters describe a slightly divergent 20-keV proton beam at the entrance to the lens.

The first step with TRACE is to evaluate the properties of the matched beam at the entrance to the RFQ. The standard approach for this, shown in Fig. 13, is to describe the initial portions of the RFQ linac as a radial matching section of length  $3\beta\lambda$  and four half cells, each of length  $\beta\lambda/4$ . The matched beam within the RFQ is determined by calculations through the four half cells (one period) of the focusing structure. The twiss parameters for this beam are shown on Fig. 13 to be  $\alpha_{twiss}=1.7912$  and  $\beta_{twiss}=0.0046$  mm/mrad. This matched beam is then "backed out" of the RFQ, as shown in Fig. 14, starting at the end of each half cell and extending to the entrance plane of the RFQ. The average of these results are taken as the descriptions of the matched beam at the entrance to the RFQ. The twiss parameters at this point are  $\alpha_{twiss}=2.250$  and  $\beta_{twiss}=0.026$  mm/mrad. This corresponds to a highly convergent beam with a diameter of 3.6 mm at the entrance to the RFQ linac.

A matrix of RFQ lens design calculations were made using the computer program TRACE. At a frequency of 425 MHz (the RFQ linac frequency), the required field strength and rf power levels are excessive. As noted earlier, there are distinct advantages in operating at a frequency that is below that of the linac. At a frequency of 100 MHz, the length of the output matching sections ( $3\beta\lambda=5.9$  cm) is excessive, forcing an increase in the lens aperture to accommodate the beam. There is a broad optimum in performance in the vicinity of 300 MHz.



I= 20.0 20.0  
W= 0.020 0.020  
EX= 122.00 122.00  
EY= 122.00 122.00

MATCHING VARIABLES  
ME MP VALUE  
50 1 -1.791  
50 2 0.005  
50 3 1.791  
50 4 0.005

MATCHING TYPE = 6  
DESIRED VALUES:  
(INPUT BEAM VALUES)  
ALPHA-X -1.791  
BETA-X 0.005  
ALPHA-Y 1.791  
BETA-Y 0.005

MISMATCH FACTORS:  
X-plane 0.000  
Y-plane 0.000

CODE: TRACE v42  
FILE: RFL2.DAT;5  
DATE: 30-AUG-90  
TIME: 14:40:51

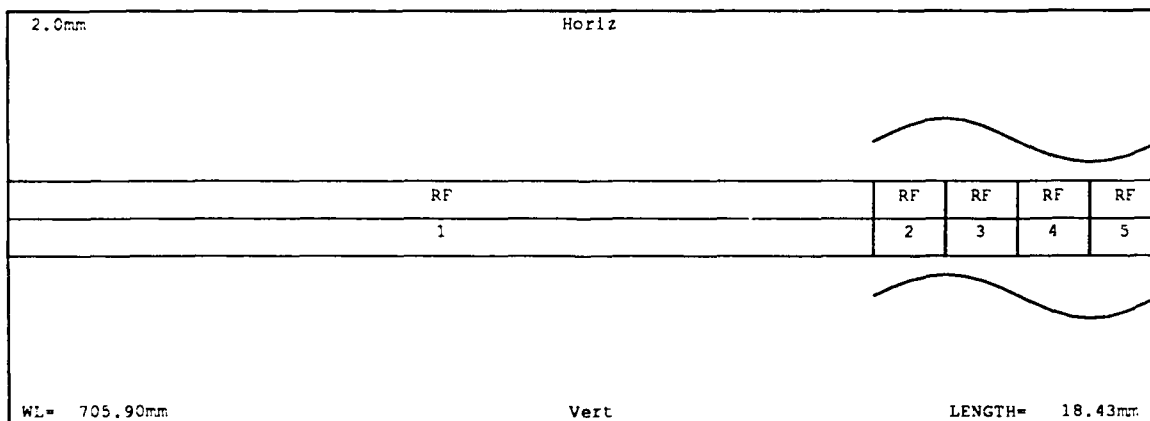
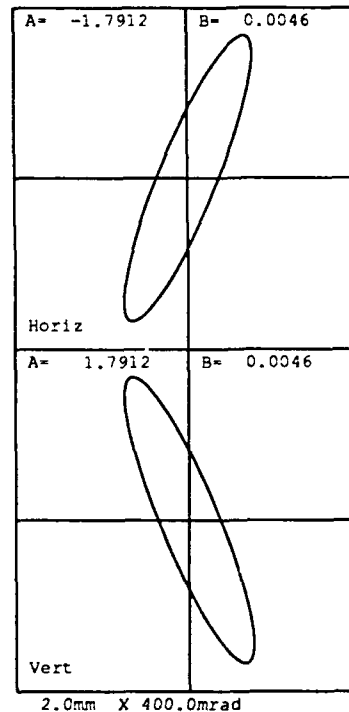
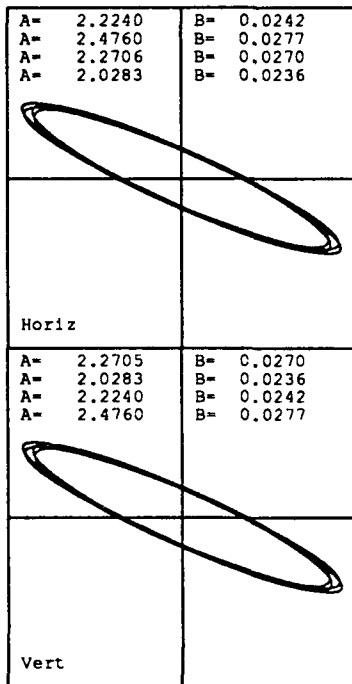


Fig. 13. TRACE Calculation to Determine Matched Beam within the RFQ Linac.



I= 20.0 20.0  
W= 0.020 0.020  
EX= 122.00 122.00  
EY= 122.00 122.00

MATCHING VARIABLES  
ME MP VALUE  
50 1 -1.791  
50 2 0.005  
50 3 1.791  
50 4 0.005

MATCHING TYPE = 6  
DESIRED VALUES:  
(INPUT BEAM VALUES)  
ALPHA-X -1.791  
BETA-X 0.005  
ALPHA-Y 1.791  
BETA-Y 0.005

CODE: TRACE v42  
FILE: RFL2.DAT;5  
DATE: 25-AUG-90  
TIME: 14:56:01

RFQ MATCHING

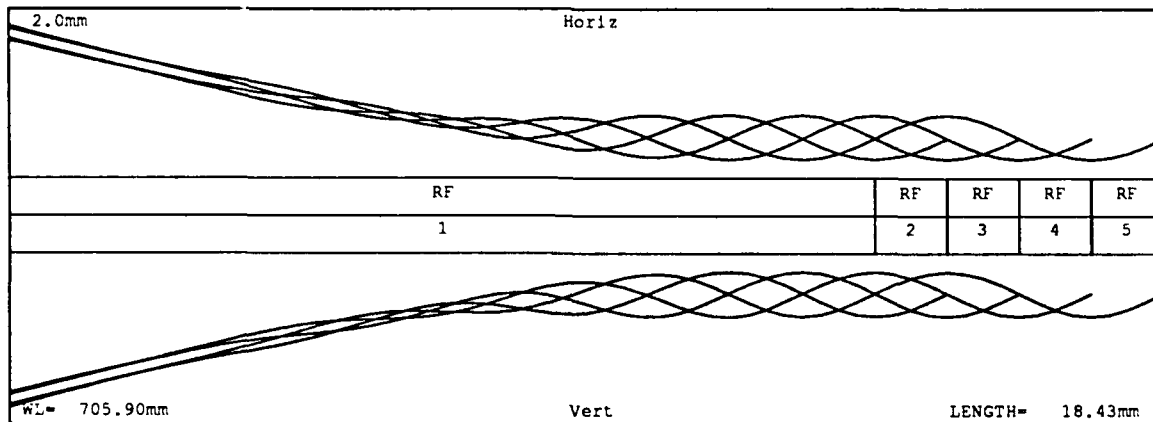
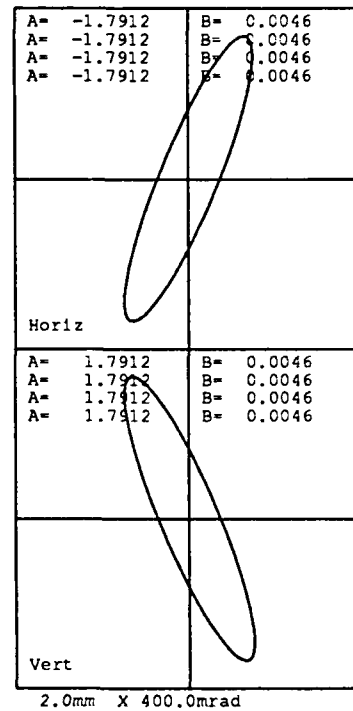


Fig. 14. TRACE Calculation to Determine Matched Beam at Entrance to RFQ Linac.

The required smooth variation in field strengths through the lens sets a minimum length for a 300 MHz lens of  $8\beta\lambda=5.2$  cm. Lengths as great as 20 cm spread the focusing to such an extent that the lens aperture must be increased to accommodate the beam. There is a broad optimum in the vicinity of  $14\beta\lambda=9.13$  cm.

The performance of a 300 MHz,  $14\beta\lambda$  RFQ lens in front of a 425 MHz RFQ linac is shown in Fig. 15 as a composite of two TRACE calculations. The separation between the RFQ lens and the RFQ linac is 1.27 cm (0.5 inches). The excitation of the lens for this calculation is  $B=1.2$ . This figure shows the results of backing the beam out from the RFQ linac through the RFQ lens to the entrance of the lens. The average twiss parameters at key locations in this composite TRACE calculation are shown below:

Location	$\alpha_{\text{twiss}}$	$\beta_{\text{twiss}}$ (mm/mrad)
Internal RFQ linac	1.7912	0.0046
Entrance to RFQ linac	2.2500	0.0260
Entrance to RFQ lens	-2.3160	1.1770

Note that the beam parameters at the entrance to the RFQ lens are very similar to those assumed at the beginning of this section ( $\alpha_{\text{twiss}}=-2.4000$ ,  $\beta_{\text{twiss}}=1.200$  mm/mrad). Thus, this calculation shows the prescribed beam focused and matched into the RFQ linac by the RFQ lens. If the beam at the entrance to the RFQ lens differs from this prescription, modest changes in lens excitations and position can reestablish the match to the RFQ for a wide range of input beam variations.

The calculated performance shown in Fig. 15 is close to the design goal for the project. The decision was made to fabricate this lens as a four-vane RFQ structure with a length of 3.5 inches (8.89 cm) and a bore radius of 2.0 cm. A first-order estimate of the transverse dimensions and electrical properties of the structure was obtained from SUPERFISH. Fig. 16 shows the triangular mesh and the resulting quadrupole electric field pattern from SUPERFISH for one quadrant of the structure. A diameter of 10 inches results in a resonant frequency of approximately 300 MHz.

The very short length-to-diameter ratio of the RFQ lens means that the resonant properties of the structure, and its rf power requirements, are heavily influenced by "end effects", which are not properly treated in the two-dimensional SUPERFISH calculations. Nevertheless, the mechanical design of the outer parts of the lens cavity and vacuum enclosure were based on these

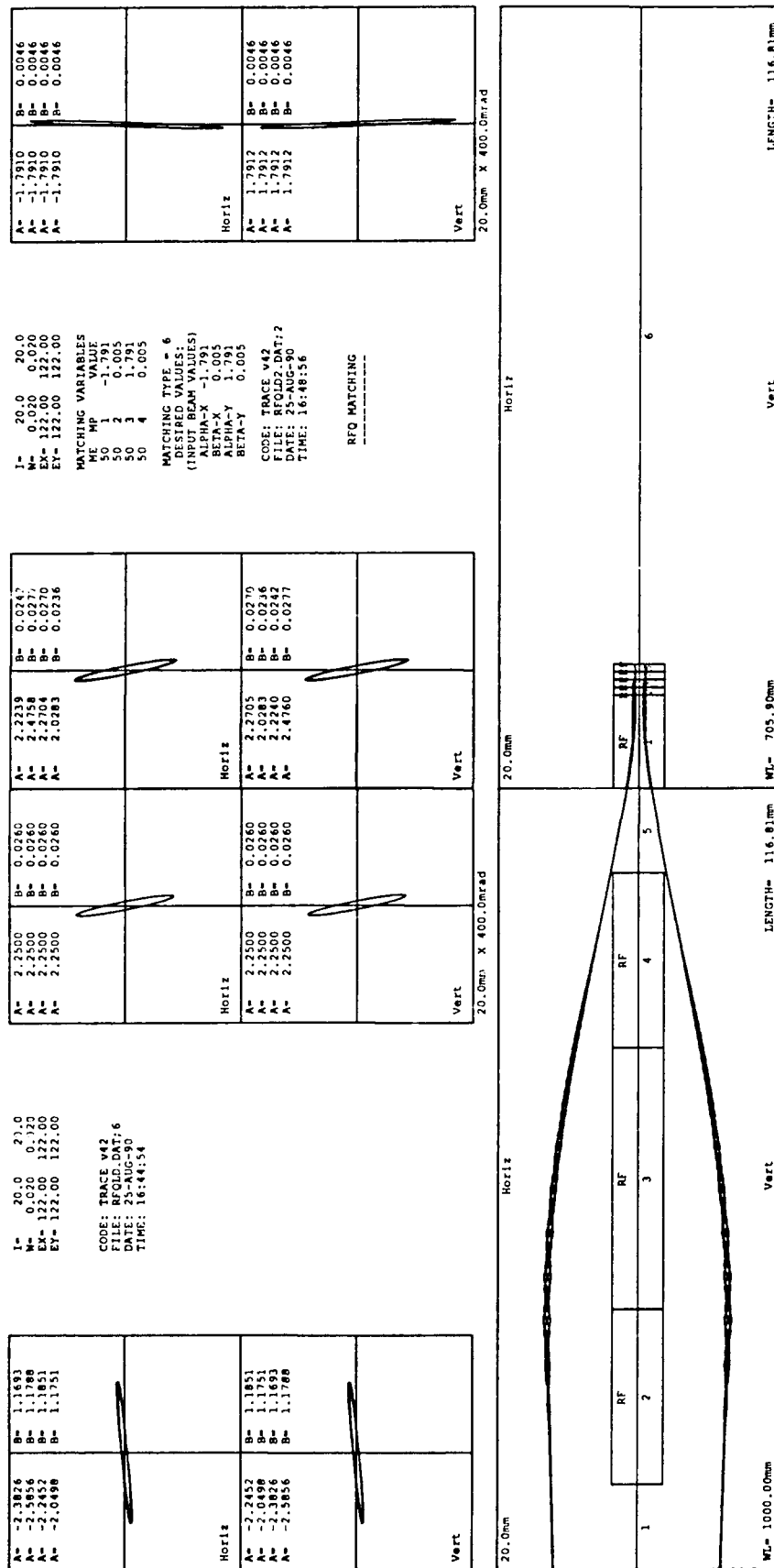
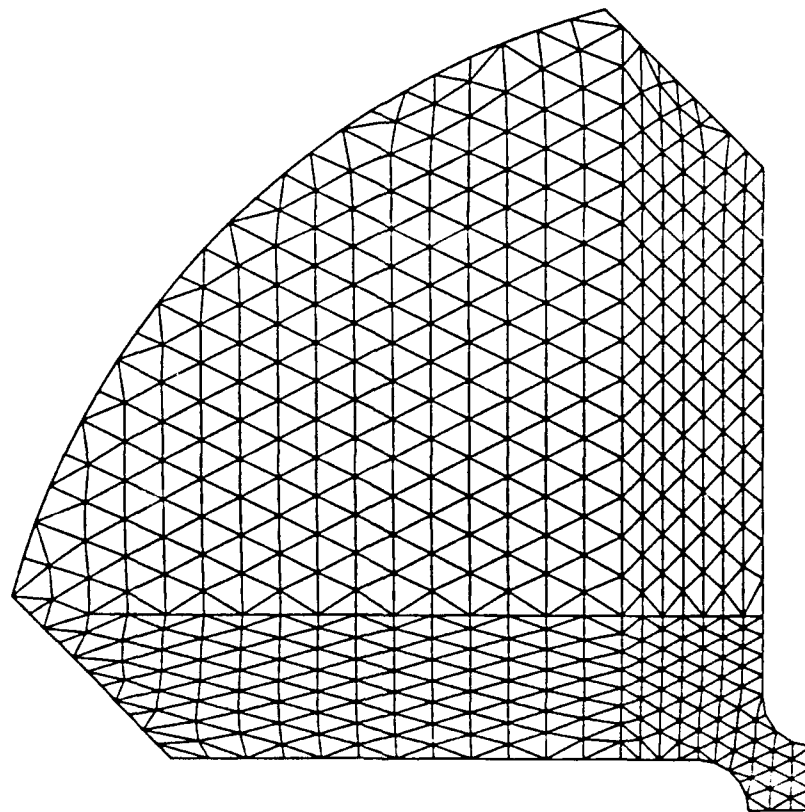


Fig. 15. Performance of 300-MHz RFQ Lens in Front of 425-MHz RFQ Linac.

SUPERFISH OUTPUT (SF04)

13:21:23 16-DEC-88



RUN NO. 206 RFQ Lens (300 MHz)

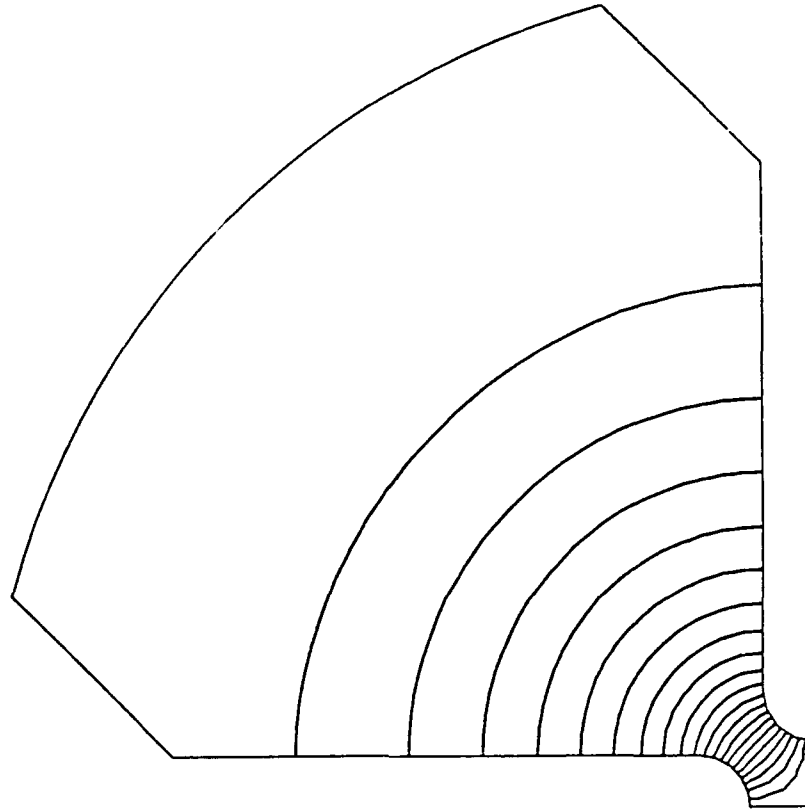


Fig. 16. SUPERFISH Mesh and Calculated Electric Fields for RFQ Lens.

SUPERFISH calculations, leaving the detailed accommodation of the end effects to be sorted out experimentally. This accommodation was to be accomplished by designing the vanes to take into account the end effects and result in a lens with the desired performance and frequency. As mentioned earlier, it was anticipated that the resonant frequency of the structure would be less than 300 MHz and simple steps could be taken to increase the resonant frequency to 300 MHz. The final design of the vanes is described in Section 7. Fabrication of these long-lead items (cavity and vacuum enclosure) was initiated to provide an enclosure for these "end effects" experiments and to permit other related systems to be designed on schedule.

The outer part of the lens cavity was constructed as a heavy-walled cylinder, 10 inches in diameter and 3.5 inches long. Four vane assemblies mount inside this cylindrical enclosure, attached to the heavy cylindrical wall by two concentric push/pull screw assemblies. The pushing screws have micrometer threads to the cavity wall and form the basis of the vane alignment system. The pulling screws serve to pull the vane bases against these alignment surfaces. Two additional push screws per vane provide fine control of the longitudinal alignment of the vane tips. Locking plates load the alignment screw threads to prevent accidental movement. The vane alignment is accomplished by simple mechanical measurements. Electrical contact between the vane bases and the cavity wall is based on flexed fins at the edges of the vane bases, which are designed to produce forces of 100 pounds/inch against the cavity wall.

The vacuum requirement for the RFQ lens is simplified by surrounding the entire lens assembly with a vacuum housing that bolts directly to the end of an RFQ linac. This arrangement allows the lens to be mounted very close to the RFQ linac and provides a small range of longitudinal adjustment to accommodate beam matching requirements.

The principal mechanical features of this design are shown in Fig. 17 (original vane geometry). Detailed mechanical designs for the major RFQ lens components are shown in Figs. 18-23.

The electrical properties of the RFQ lens, evaluated by SUPERFISH, are summarized on the SRO5 output shown in Fig. 24. The SUPERFISH normalization corresponds to a lens excitation of  $B=1.34$ . When renormalized to  $B=1.2$ , the vane-to-vane voltage is 112 kV, the surface electric field on the vane tip is 11.2 MV/m, the maximum surface electric field is 13.9 MV/m (0.81 Kilpatrick), the power dissipation is 79.3 kW/m or 7.05 kW, the stored energy is 0.616 J/m or 0.548 J, and the  $Q$  is 14,649. One must note, however, that these are first-order estimates of the electrical parameters based on the two dimensional SUPERFISH calculation.

- Simple to Fabricate and Assemble.
- Mounts directly on RFQ Linac.
- Longitudinal Lens-Position Adjustment.
- Very Close Lens-to-RFQ Linac Spacing.
- External Vacuum Can.
- Could Accommodate Vacuum Pump.
- Dedicated Close-Coupled RF Power.
- Accommodated Beam Dynamics Spools.

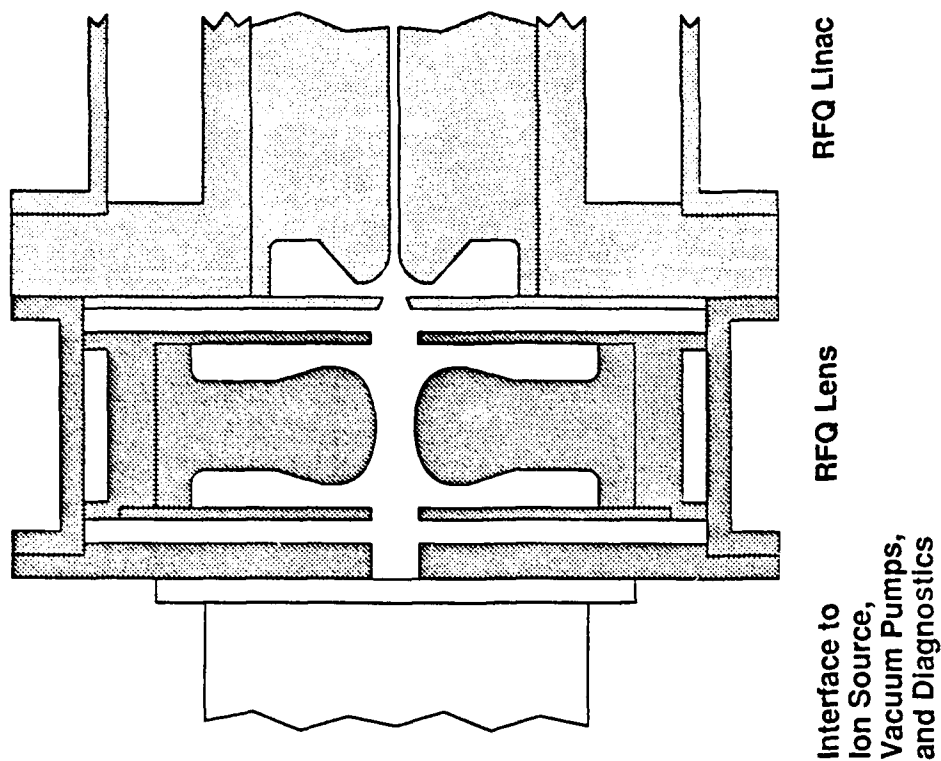
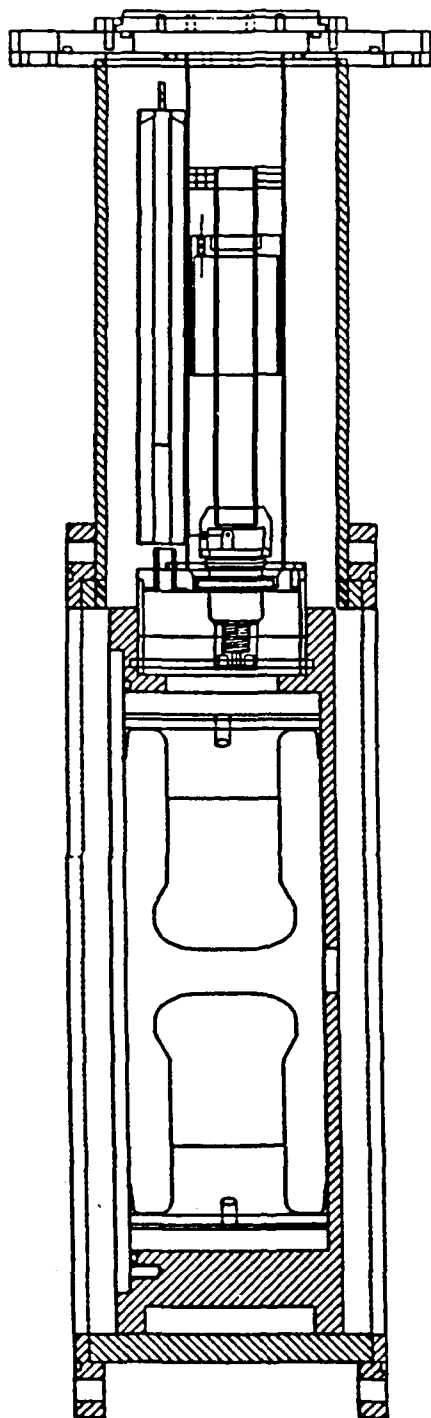


Fig. 17. RFQ Lens Mechanical Features.

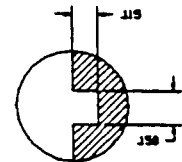
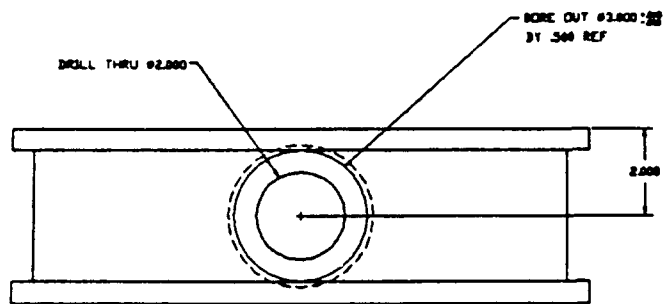




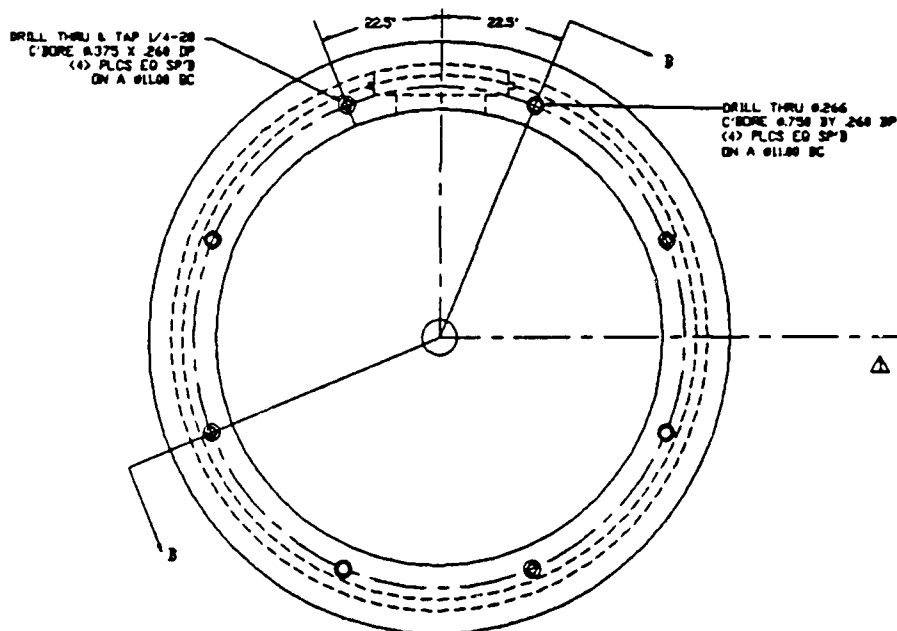


DATE	10/1/81	BY	W. J. B.	REV	1	QTY	1	UNIT	ASSEMBLY	DESCRIPTION	RFQ LENS AND CCRF ASSEMBLY
DESIGNED BY	W. J. B.	CHECKED BY	W. J. B.	DATE	10/1/81	QTY	1	UNIT	ASSEMBLY	DESCRIPTION	RFQ LENS AND CCRF ASSEMBLY
APPROVED BY	W. J. B.	DATE	10/1/81	QTY	1	UNIT	ASSEMBLY	DESCRIPTION	RFQ LENS AND CCRF ASSEMBLY		
REVISIONS											
1	10/1/81	W. J. B.	1	ASSEMBLY	RFQ LENS AND CCRF ASSEMBLY						

Fig. 19. RFQ Lens and CCRF Assembly (Side View).



DETAIL D  
SPRING RING GROOVE



RIGHT VIEW

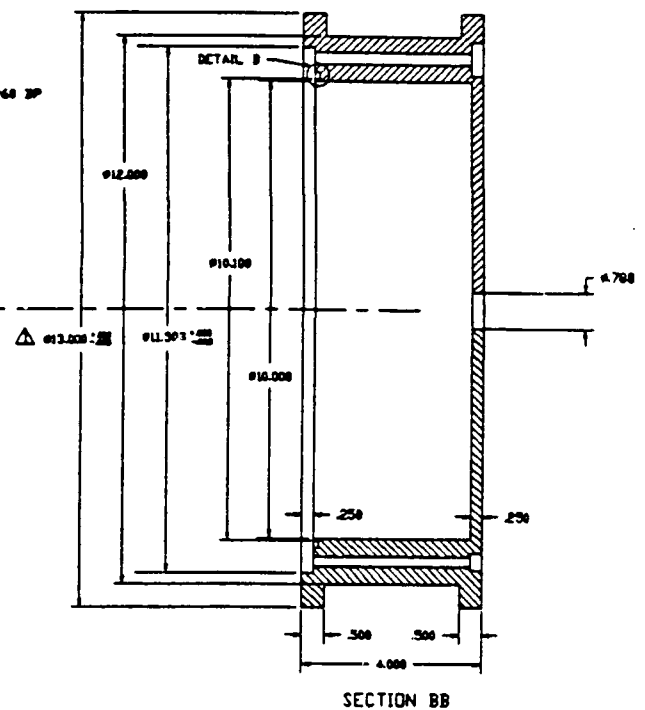
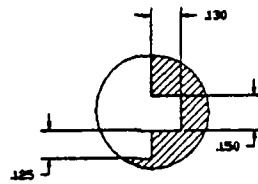
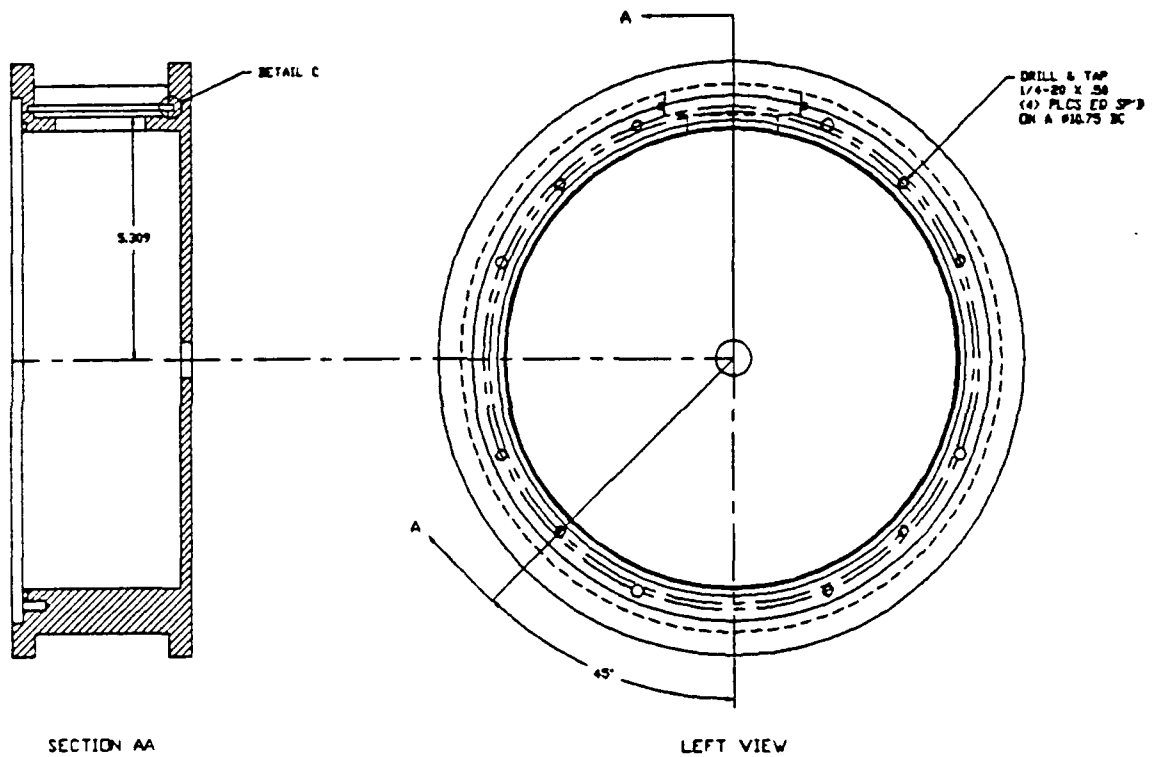


Fig. 20. RFQ Lens Body (Section BB).

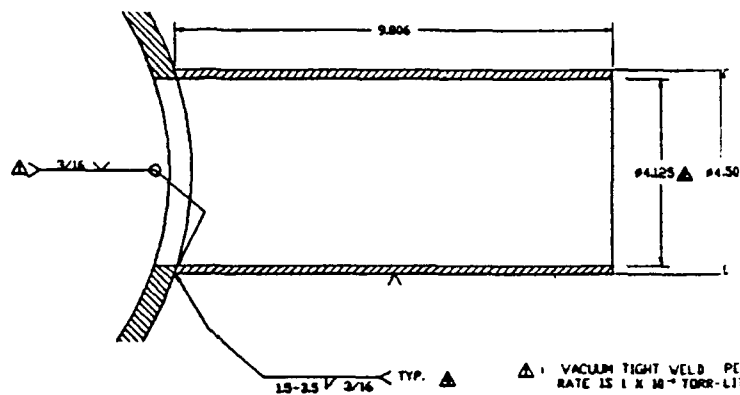
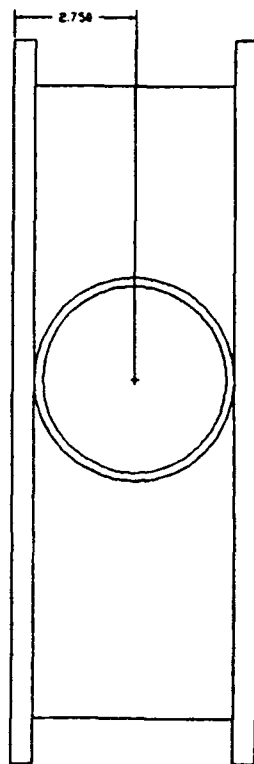


DETAIL C  
-----  
SPRING RING GROOVE



NOTE:  
ENTIRE PIECE TO BE MACHINED OUT OF ONE ALUMINUM BLOCK.  
△ DIMENSION TO PROVIDE A SLIDING FIT INTO VACUUM HOUSING (04-20270).

Fig. 21. RFQ Lens Body (Section AA).

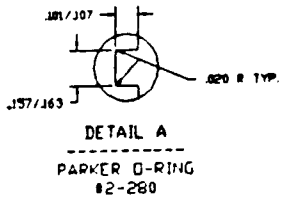
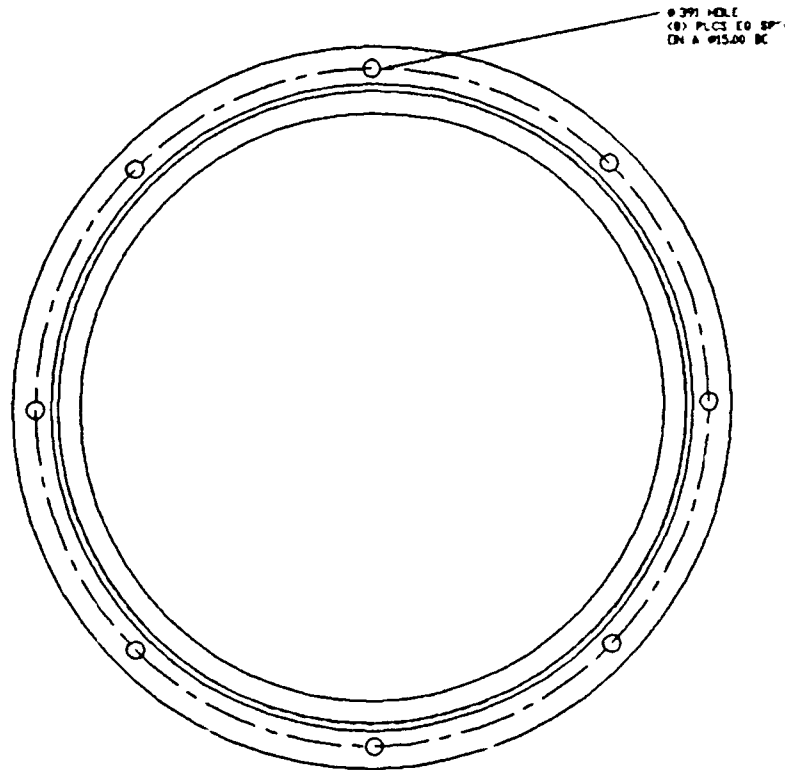
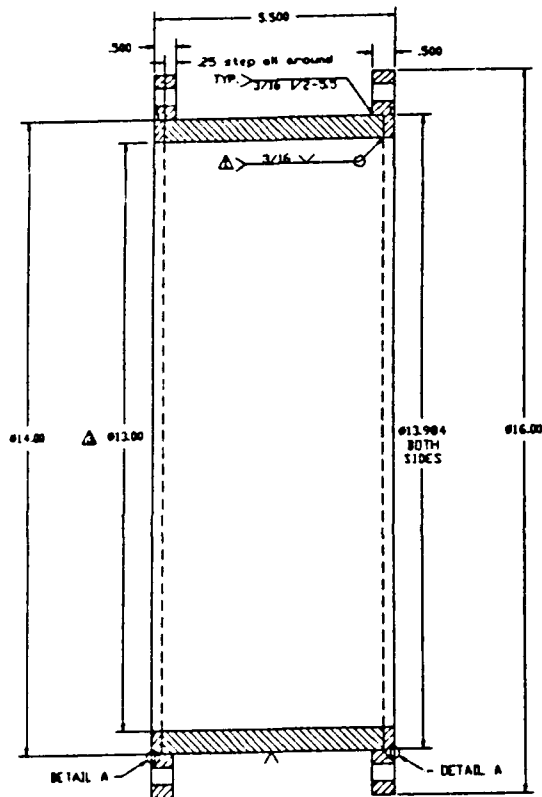


RF FLANGE

- △: VACUUM TIGHT WELD. PERMISSIBLE LEAK RATE IS  $1 \times 10^{-10}$  TORR-LITER/SEC
- △: BORE OUT TO THIS DIMENSION AFTER WELDING TO HOUSING.
- △: BORE OUT TO 0.003 IN AFTER WELDING COMPLETED.
- △: WELDS TO BE POSITIONED SO AS NOT TO INTERFERE WITH FLANGE BOLT HOLES.

BY	DATE	PART OR IDENTIFYING NO.	NOMENCLATURE OR DESCRIPTION	MATERIAL SPECIFICATION
PARTS LIST				
UNLESS OTHERWISE SPECIFIED DIMENSIONS ARE IN INCHES TOLERANCES ARE DECIMALS ANGLES 3/16 0.005 1°		<div style="display: flex; justify-content: space-between;"> <div> <p>CONTRACT NO.</p> <p>APPROVALS</p> <p>DRAWN SRS</p> <p>CHECKED</p> <p>ISSUED 8 212</p> </div> <div> <p>DATE</p> <p>8-18-91</p> </div> <div> <p><b>SATE</b> <small>Space Applications International Corporation</small></p> <p><b>RFQ LENS VACUUM HOUSING</b></p> </div> </div>		
MATERIAL AL		<div style="display: flex; justify-content: space-between;"> <div> <p>SIZE D</p> <p>SCALE 1/2</p> </div> <div> <p>DWG. NO. 04-20270</p> </div> <div> <p>REV</p> </div> </div>		
NEXT ASSY	USED ON	SHEET		
APPLICATION		DO NOT SCALE DRAWING		

Fig. 22. RFQ Lens Vacuum Housing (RF Flange).



## INITIAL VACUUM TANK

Fig. 23. RFQ Lens Vacuum Housing (Vacuum Tank).

```

* * * INPUT DATA FOR RUN * * *
RUN                **RFQL300.DAT**
TITLE
RFQ Lens (300 MHz)
MESHX  .3 3 .6 12.477
MESHY  .3 1003 .6 1012.477
NSEG 10
XSEG 0 .8 .8 3.277 9.122 12.477 10 1.8 1 0
YSEG 1001 1001.8 1010 1012.477 1009.122 1003.277 1000.8 1000.8 1000 1000
CSEG 0 .8 0 0 -12.9 -12.9 0 0 .8 0
FREQ 300
DRIVE 5
BOUNDARY 1 0 1 0
POWER 2 3 4 5 6 7 8 9
MESHMAP
BEGIN
END

```

\* \* \* SUPERFISH RESULTS FOR RFQ \* \* \*

RADIUS OF TOROID	=	10.000	m
CIRCUMFERENCE OF TOROID	=	62.832	m
FREQUENCY (STARTING VALUE = 300.000)	=	300.202	MHz
ASCALE (NORMALIZATION FACTOR)	=	21732.9	
MAX ELECTRIC FIELD ON BOUNDARY	=	15.567	MV/m
MAGNETIC FIELD ON OUTER WALL	=	5730	A/m
POWER DISSIPATION/M	=	0.0989	MW/m
STORED ENERGY/M = 0.00004859*V(kV)**2	=	0.7684	J/m
QUALITY FACTOR (Q)	=	14649	
AVERAGE GRADIENT	=	1257.5	MV/m/m
RFQ APERTURE	=	1.0000	cm
VANE-TO-VANE VOLTAGE	=	125.751	kV
SHUNT IMPEDANCE = 8313699/F**1.5/A**2	=	1598.36	MOhm/m
EZ ON THE AXIS (MV/m) FROM K = 1 TO 5.			
0.000 2.442 6.172 10.101 14.085			
AT Z VALUES OF (cm)			
0.000 0.197 0.500 0.803 1.060			

Fig. 24. RFQ Lens Electrical Properties Evaluated by SUPERFISH (SFO5).

The RFQ lens requires a source of rf power. SAIC is currently developing a family of close-coupled rf (CCRF) power systems, which promise many advantages over the conventional rf power systems. They are designed to mount directly on the side of the resonant load and operate in an extension of the resident vacuum system, thus eliminating many components of conventional rf power systems such as rf output resonators, transmission lines, and vacuum windows.

One of these CCRF units, based on the Eimac Y-690 Planar Triode and capable of peak rf power in excess of 20 kW, was used to power the RFQ lens. This unit, shown in Fig. 25, mounts inside the tubular extension to the vacuum housing, shown in Fig. 26, and couples directly to the RFQ lens fields.

The CCRF power amplifier is configured as a grounded-grid amplifier. The cathode is biased 40 volts positive with respect to ground by a Zener diode. The anode and cavity coupling loop operate at an anode potential of about 6 kV. The anode is cooled by water which flows to and from the anode cap through the loop. The rf currents are shorted to ground through an rf bypass capacitor that is an integral part of the design.

Three chassis of the rf drive chain are shown in Figs. 27 and 28. The top unit (in both figures) is a collection of broad-band, solid-state amplifiers that amplify one-milliwatt input to an output power of 25 W. The latter stages of this collection are pulsed at the lens duty factor of one percent. The lower two amplifiers in these figures are strip-line amplifiers based on the Eimac 8940 Planar Triode. The middle unit takes an input of 25 W and amplifies it to 350 W. The lower unit takes an input power of 350 W and delivers 2 kW to the output. This power is transmitted through an ordinary RG-58 coax cable and a hermetically sealed SMA connector to the CCRF power amplifier inside the RFQ lens vacuum housing.



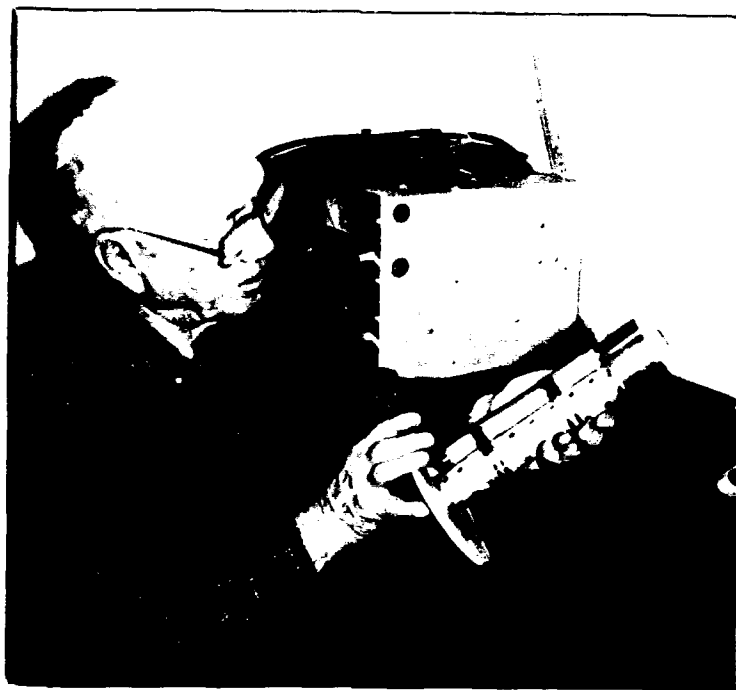


Fig. 25. The CCRF Power Amplifier and Designer.

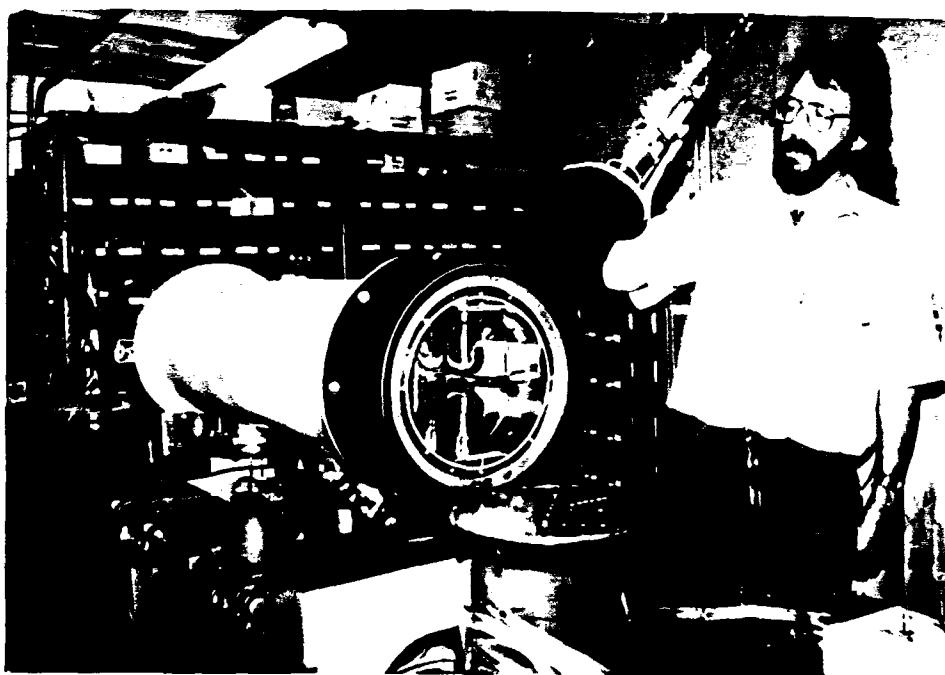


Fig. 26. Vacuum and Power Test Configuration for the RFQ Lens.

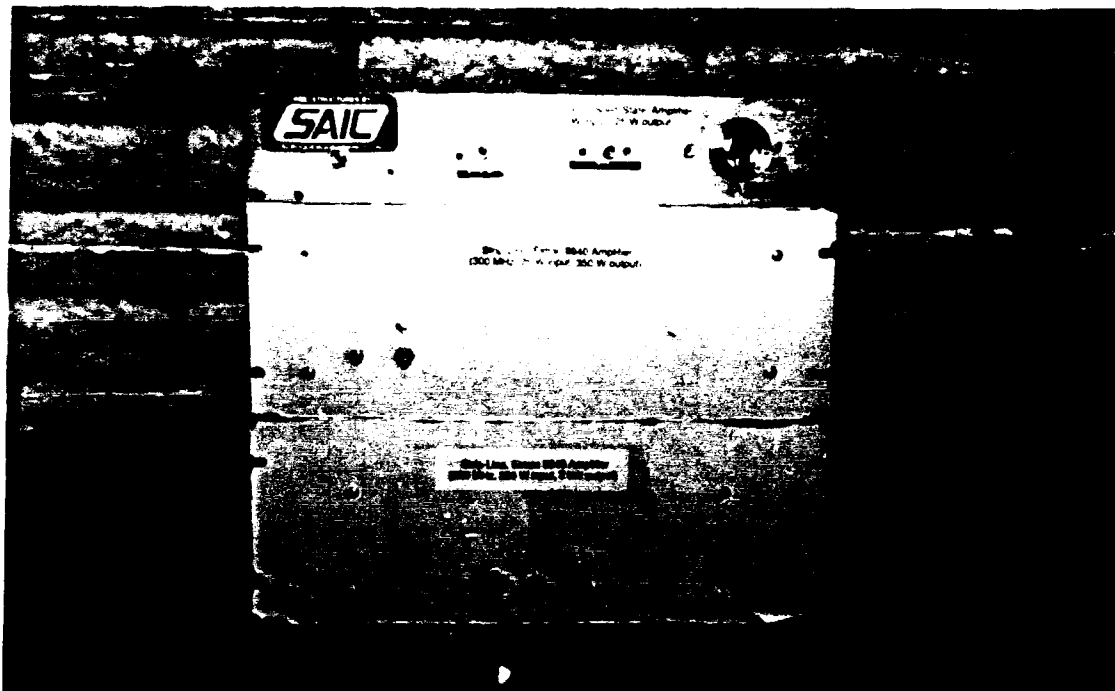


Fig. 27.  
CCRF Drive  
Power Chain  
(Front View).

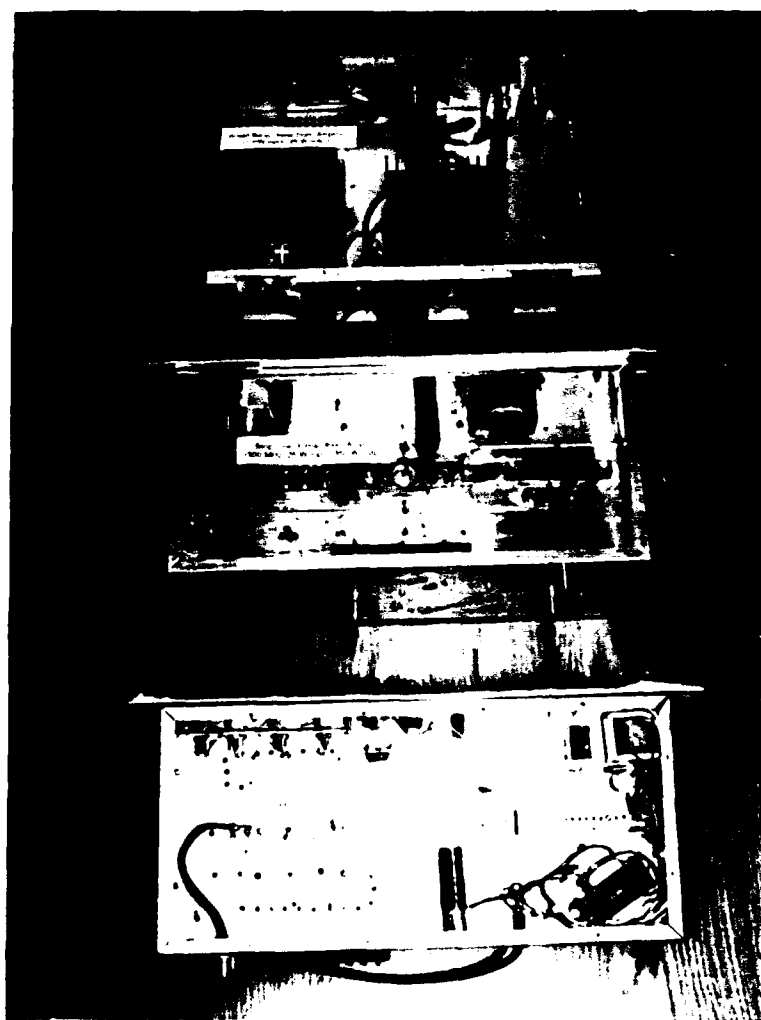


Fig. 28.  
CCRF Drive  
Power Chain  
(Bottom View).

## 7. PRE-BEAM TESTS AND FINAL VANE DESIGN FOR THE RFQ LENS SYSTEM

Tests were performed at SAIC before proceeding to the beam tests at Fermi National Accelerator Laboratory (FNAL) in order to check out and tune the lens and thereby maximize the utility of valuable time at FNAL. In addition, the vane design had to be finalized, taking into account the three-dimensional end effects described earlier. In order to experimentally investigate different vane geometries, wooden vanes covered with aluminum tape were used as a source of readily changeable geometries together with the outer portions of the cavity that had already been fabricated. The lens cavity, loaded with the vanes that we had expected to use, resonated at 588 MHz; substantially higher than the desired operating frequency of 300 MHz.

Since the magnitude of the rf frequency has a big effect on the RFQ focusing, it was important to understand this discrepancy and develop an approach to achieve the desired resonant frequency of 300 MHz. Although not planned or budgeted for this project, three-dimensional ARGUS calculations were performed for this geometry, which confirmed the experimentally observed resonant frequency.

We had expected the end effects in the RFQ lens cavity to reduce the resonant frequency of the actual structure relative to the SUPERFISH prediction. These expectations were based on our opinions that:

- 1) the shortening of the vanes to allow room for the magnetic fields to loop around the ends of the vanes should increase the inductance of the circuit, and
- 2) the presence of the end wall near the vane tips should increase the capacitance of the circuit.

Both of these end effects should lower the resonant frequency of the structure. Nevertheless, just the opposite happened.

This experimental observation has made us consider another, possibly more powerful, three-dimensional effect. The end effects may have wrapped the magnetic fields tightly around the vane tip supports, causing them to operate as quarter-wave resonators. A quarter wavelength at 588 MHz is 5 inches; just the effective length of the original vanes.

Had the end effects lowered the frequency, as we expected, it would have been relatively simple to raise the resonant frequency by building bulkier RFQ vanes to put inside the outer envelope of the cavity. The inverse is not true. It is considerably more difficult to lower the resonant frequency of a cavity of fixed outer geometry than it is to raise it.

We were left with two options to achieve the desired operating frequency for the RFQ lens: one was to fabricate new, larger-diameter lens and vacuum enclosures, and the other was to modify the geometry of the vanes sufficiently to load the resonant frequency of the cavity down to 300 MHz. In the interest of budget and schedule, the latter option was chosen.

The resonant frequency of the RFQ lens was lowered to 300 MHz by narrowing the vane bodies to rods (higher inductance) and adding tabs to the vane tips (higher capacitance to the end wall). For purpose of comparison, a section of the RFQ lens is shown in Fig. 29 with both the original (top) and modified (bottom) vane geometries.

These changes, however, resulted in a significantly lower rf efficiency and a lower Q for this lens, with a significant increase in the rf power required to achieve the desired focusing strength from the lens. Since we anticipated having some excess rf power, we decided to proceed with a beam test of this lens unit as scheduled.

The assembled RFQ lens, with one cover plate removed, is shown in Fig. 1. The "vane tips" are circular arcs, supported from base plates by radial rods of approximately one-half inch in diameter. Four such assemblies are mounted inside a heavy-walled cylindrical cavity, 10 inches in diameter and 3.5 inches long. The cylindrical cavity and vane bases are made of aluminum and copper-plated for electrical conductivity. Each base plate is attached to the heavy cylindrical wall by two concentric push/pull screw assemblies. Electrical contact between the vane bases and the cavity wall is based on flexed fins at the edge of the vane bases. The mode spectra, Q measurement, and distribution of fields on the four vane tips are shown in Fig. 30. The unwanted dipole modes are at approximately 325 MHz, well separated from the desired quadrupole mode at 300 MHz. This well-spaced separation of the dipole and quadrupole modes means that the alignment of the vanes is not critical and can be accomplished by simple mechanical measurements. The unloaded Q of the cavity is 2600; a factor of 5 lower than the SUPERFISH prediction of 14,649.

The RFQ lens is powered by a close-coupled rf (CCRF) power system. Matching of a CCRF power system to a resonant cavity presents a problem for which there is little experience. The output impedance of the Eimac Y-690, at full power (20 kW), is about 800 ohms. Conventional rf power systems, in this frequency range, deliver their power through coaxial transmission lines with an impedance of about 50 ohms. The higher impedance of the CCRF system suggests the need for a considerably larger coupling loop. Since loop impedance varies directly as the square of the loop area, one would expect the CCRF loop to be about four times the linear dimensions of the conventional, 50- $\Omega$  loop. A considerable effort was expended to find a generic 800- $\Omega$  loop for the RFQ lens cavity, independent of the actual CCRF hardware, using a network analyzer. This

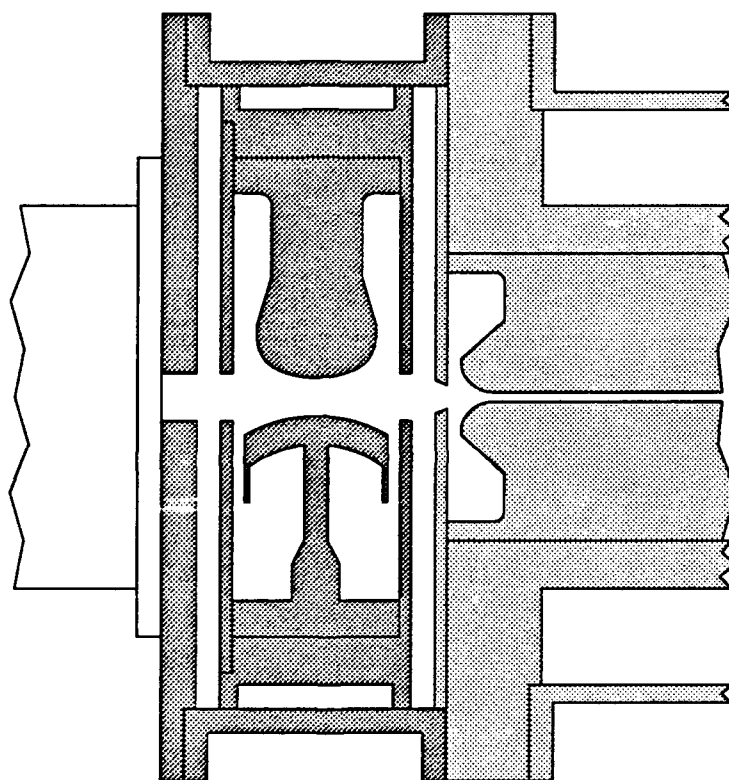


Fig. 29. RFQ Lens with Original (Top) and Modified (Bottom) Vane Geometries.

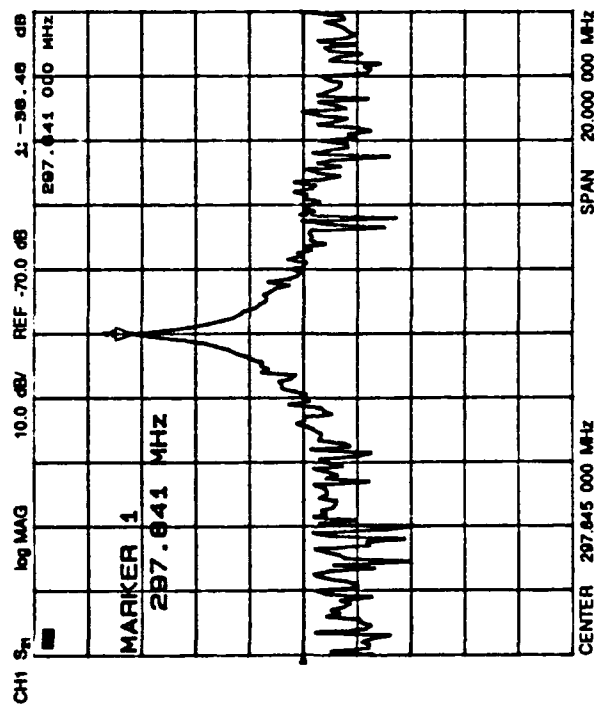
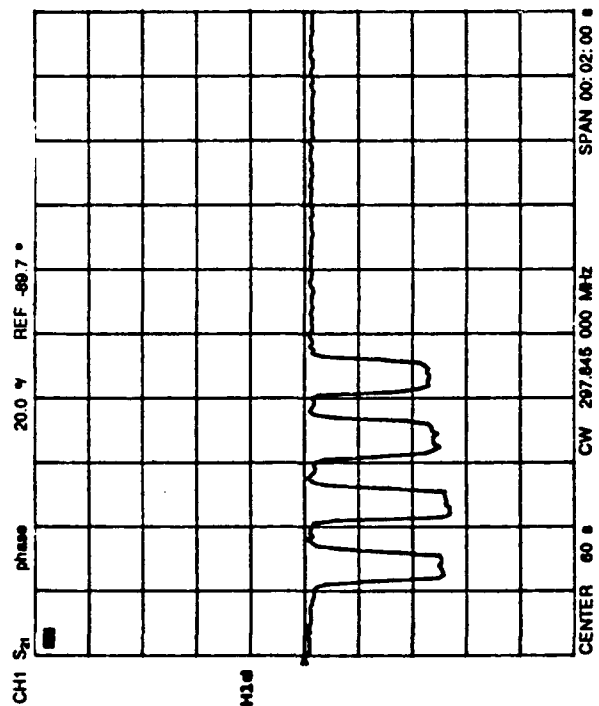
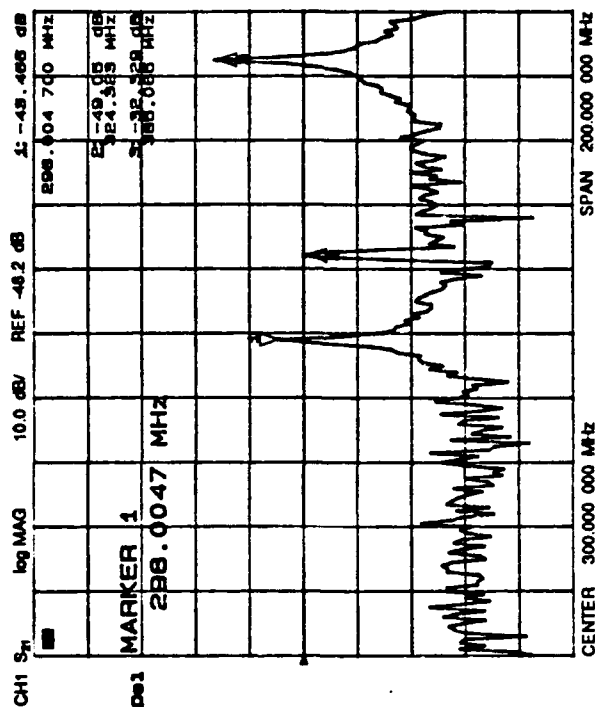
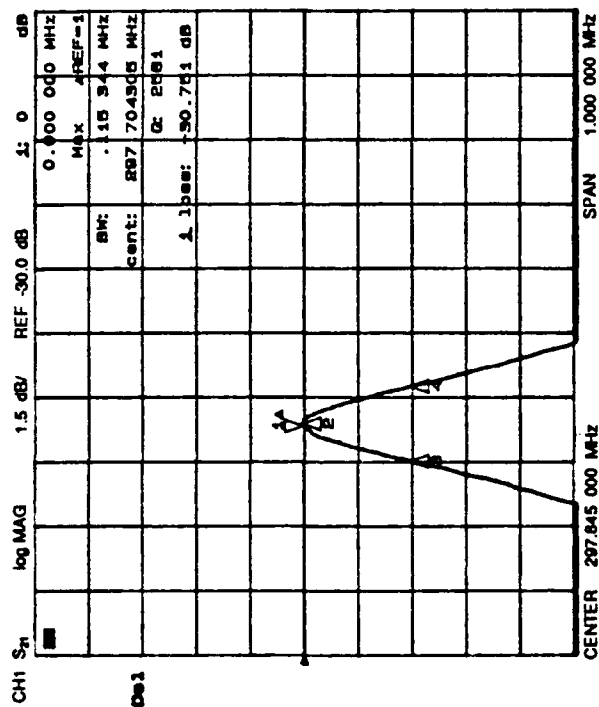


Fig. 30. RFQ Lens Mode Spectra, Q Measurement, and Field Distributions.

proved to be futile, as the details of the CCRF hardware contribute the majority of the needed impedance.

The magnetic fields surrounding the anode and anode cap have a large effect on the impedance seen by the amplifier. Furthermore, the impedance of the planar triode varies with excitation. The goal, of course, is to achieve high efficiency power transfer from the tube to the cavity at peak excitation. Since the cavity can only accept peak excitation under vacuum conditions, the final adjustments of the CCRF coupling geometry can be made only under these awkward conditions. Fortunately, the CCRF amplifier and coupling loop are designed so that they can be rotated to change the effective coupling to the RFQ lens while under vacuum operating conditions.

The RFQ lens system was set up under vacuum conditions, and tuned up for optimum performance. Several water-cooled coupling loops were fabricated and tested. The optimum performance was achieved with an effective loop area of about 0.4 square inches (loop area of about 1.2 square inches, rotated to 70 degrees from maximum coupling). Under these conditions, 26 kW of rf power were delivered to the RFQ lens cavity in response to a net rf drive power of 1300 W (forward power of 1320 W and reflected power of 20 W) and a DC input power of 39 kW (6.5 kV times 6 A). These data suggest an excellent match on the input side of the CCRF amplifier ( $V_{SWR} = 1.29$ ), excellent gain for a single stage of amplification (power ratio of 20, or 13 db), and an overall power efficiency of 67%. Both the grounded-grid circuit and the close-coupled arrangement contribute to this excellent performance.

The RFQ lens and associated systems were then packed in cartons and shipped to FNAL for a test of their performance on a 20 keV proton beam.

## 8. BEAM TESTS AT FERMI NATIONAL ACCELERATOR LABORATORY

A work-for-others agreement was negotiated with Fermi National Accelerator Laboratory (FNAL) on April 10, 1990 "for the purpose of assembling an RFQ lens on a Fermilab ion source test bench to study its operations and focusing properties for a period of no more than two weeks". It was agreed that SAIC would compensate the laboratory an estimated \$5,000 for this access and other personnel and equipment support.

The principal technical contact at Fermilab was Chuck Schmidt, head of the Linac Department at Fermilab. The ion source test stand was in the Preaccelerator R&D Laboratory in the basement of the linac building, attended by technicians Ray Hren and Jim Wendt. Assistance in installation and operation of beam diagnostic equipment and display and interpretation of beam diagnostic data was provided by John Palkovic, Elliott McCrory and Chuck Schmidt. The SAIC team consisted of Don Swenson and Steve Schmidt.

The ion source test stand at Fermilab consists of a duoplasmatron ion source mounted on one side of a large aluminum box with many large access ports. The box and one access port were large enough to allow the RFQ lens and its CCRF power system to be installed inside the box close to the output of the ion source. The beam emittance measuring probe, which mounts on one of the side ports, was modified so that it could measure the emittance of the beam close to the output of the RFQ lens. An assembly of two viewing screens, one Faraday cup, and a glass window, through which the viewing screens could be observed, were installed downstream from the RFQ lens and beam emittance probe. This experimental arrangement is illustrated in Figs. 31-35.

Three chassis of the rf drive chain and two Fermilab power supplies were mounted in a rack, interconnected, and brought into operation to produce 2 kW of pulsed rf power to drive the final CCRF power amplifier. Initially, one amplifier of the drive chain was weak, reducing the maximum drive power to 1.6 kW. For the last day of the experiment, the weak tube was replaced, and the maximum drive power returned to the design value of 2 kW.

On the third day of the experiment, all systems were ready for beam tests. The ion source was turned on to produce a 50-mA, 20-keV proton beam with an 80- $\mu$ s pulse length and a 15-Hz repetition rate. The RFQ lens was powered to a level of about 15 kW with a 100- $\mu$ s pulse encompassing the beam pulse at the same repetition rate. The divergent proton beam flooded the RFQ lens aperture with a few milliamperes passing through the lens to the Faraday cup. Uniform beam spots, approximately the diameter of the lens aperture, were seen on both viewing screens. The emittance probe showed a diverging beam in the horizontal phase space with the RFQ lens turned off.



**Test Location:** Ion Source Test Stand at Fermilab

**Ion Beams:**

H<sup>+</sup> and H<sup>-</sup>

**Energies:**

20 - 40 keV

**Currents:**

0 - 50 mA

**Configuration:**

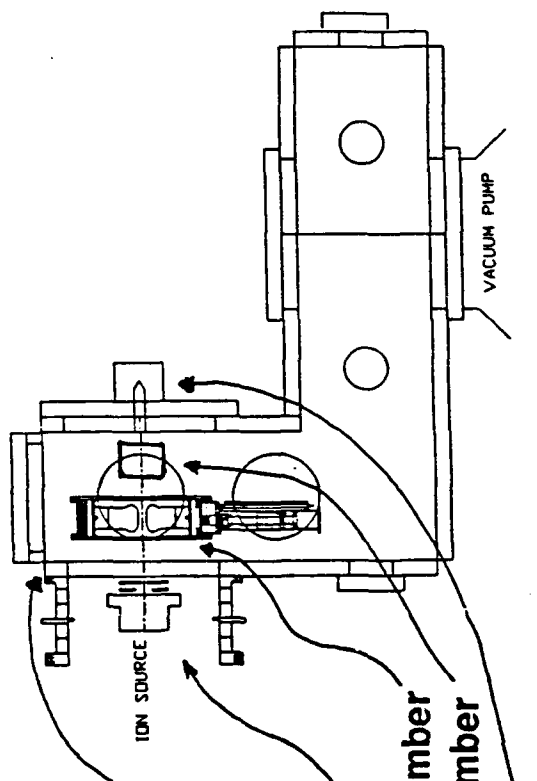
Large Test Chamber

Ion Source on One Flange

RFQ Lens Mounted Inside Chamber

Emittance Scanner Inside Chamber

Beam Stop on Other Flange



**Beam Control:**

Energy, Current, Pulse Length, Repetition Rate

Twiss Parameters (Extraction & Acceleration Potentials)

**Lens Control:**

RF Excitation

Lens Position

**Beam Diagnostics:**

Emittance Scanner

Viewing Screen

Fig. 31. RFQ Lens Test Experimental Configuration.

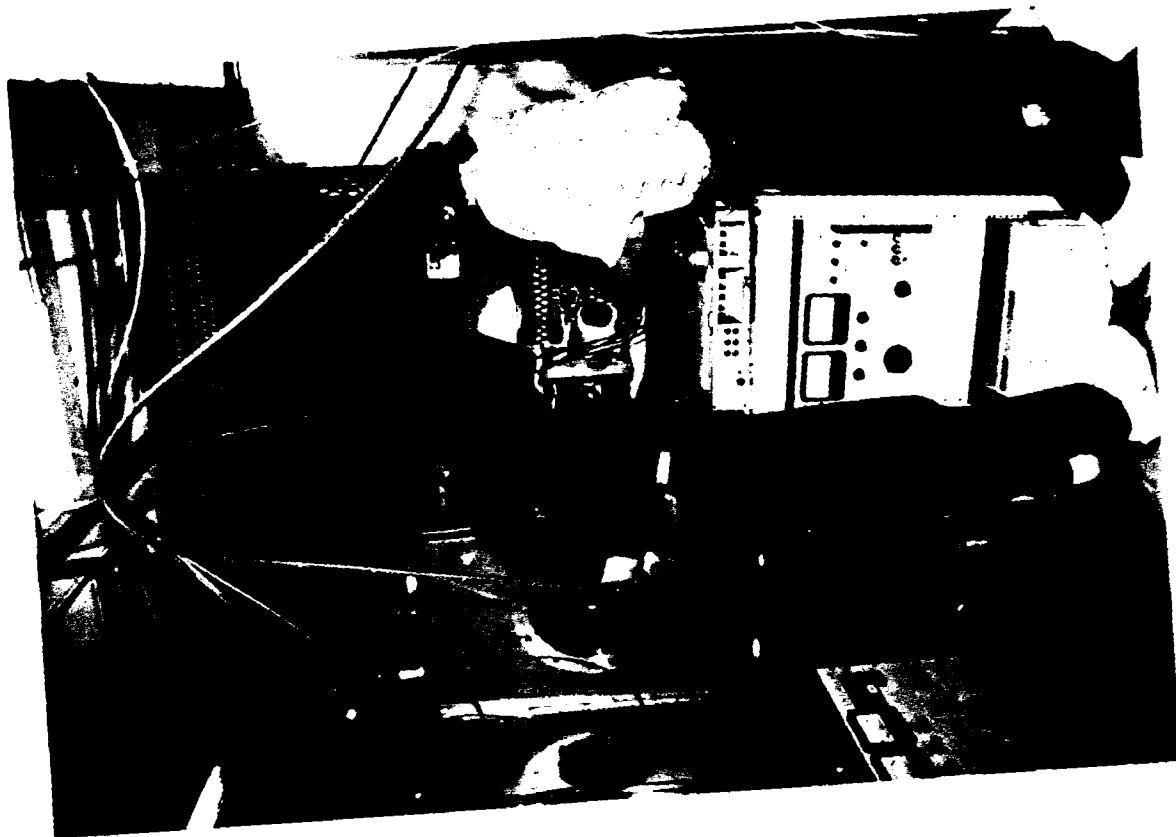


Fig. 33. John Palkovic and Steve Schmidt  
Installing Emittance Scanner.



Fig. 32. Steve Schmidt Installing RFQ Lens  
in the Test Stand.

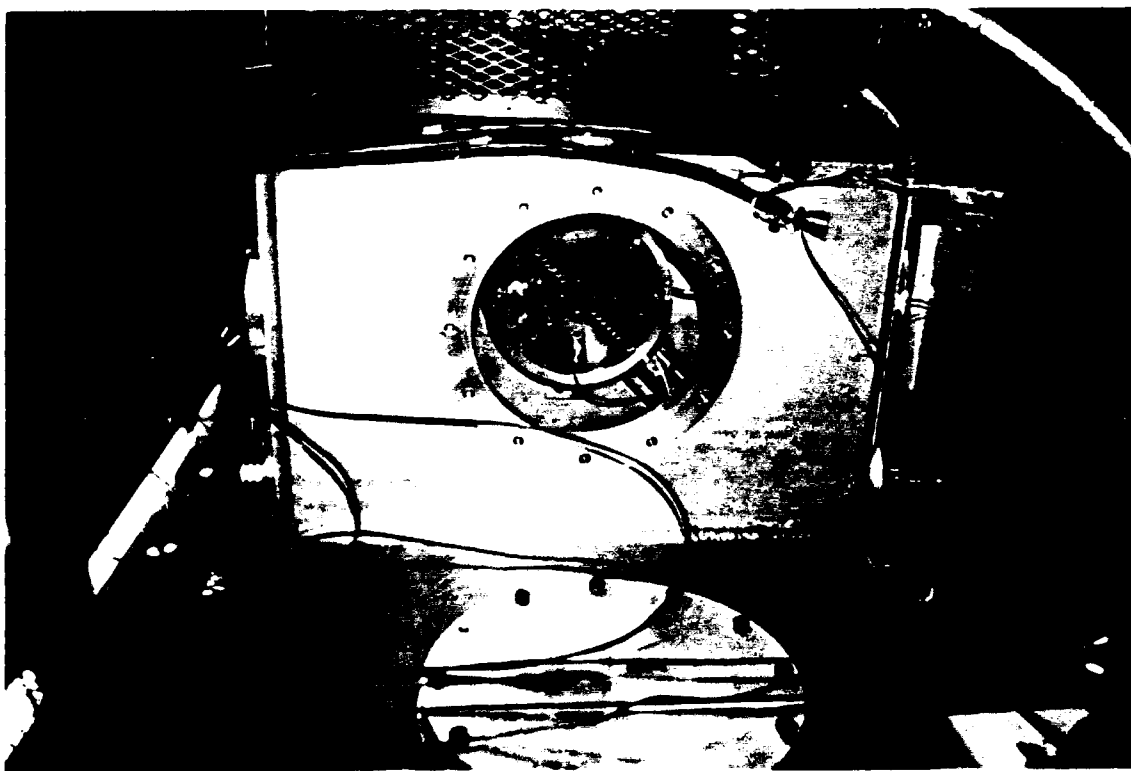


Fig. 34. RFQ Lens in Test Stand as Seen  
Through Viewing Screen Port.

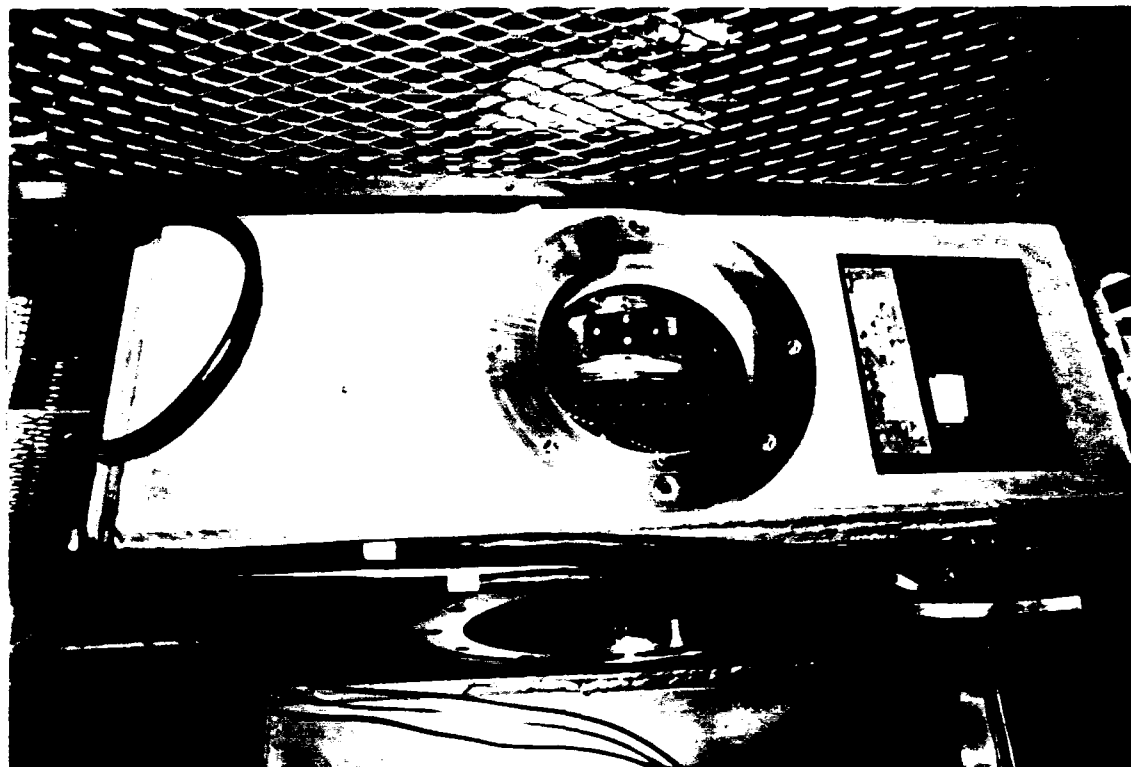


Fig. 35. RFQ Lens in Test Stand as Seen  
Through Emittance Scanner Port.

Beam observations were made using all available diagnostic devices with the RFQ lens both off and on. The emittance measurement, which would normally be the keenest indication of focusing, was difficult to interpret because of a strong electrical interference between the rf power for the lens and the emittance scanner; whenever the RFQ lens was on, the majority of beam data channels were saturated. Nevertheless, on some occasions, some traces of beam were seen through the rf induced noise. An emittance plot of the beam obtained with the lens off is shown in Fig. 36 and, for completeness, a plot with the lens on, is shown in Fig. 37. No evidence of focusing was seen in either the Faraday cup signal, the viewing screen spots, or the emittance measurement.

We knew that we were short on rf power and that the rf efficiency of the lens was less than it should have been. Nevertheless, we had expected to see some evidence of focusing and had expected to use these data to calibrate our rf power requirements. In lieu of these data, we set about to calibrate our rf power requirements through other means.

The RFQ lens was removed from the test stand and taken to a microwave measurements laboratory at Fermilab. An electric probe was fabricated whose calibration could be calculated. This probe was installed so as to sample the electric field from the vane tip. A small magnetic probe was fabricated and installed so as to sample the magnetic field on an end wall opposite one of the vane tip supports. The RFQ lens cavity was excited and the signals from these two probes were recorded. These data are sufficient to calibrate the monitor loop so that we could accurately measure the vane tip potential.

While the RFQ lens was in the microwave measurements laboratory, we verified that the rf cavity mode that we had been using in the beam tests was indeed the rf quadrupole mode, supporting our earlier finding that the dipole and quadrupole modes are well separated in frequency. The field distribution in the region between the vane tips was very much as expected.

On the fourth day of the experiment, the RFQ lens was re-installed in the test stand and, upon excitation to the 16 kW level, the newly calibrated monitor loop indicated that we had a vane-to-vane voltage of 28 kV, corresponding to a B-value of 0.3, which is a factor of four below the design value.

Subsequent TRACE calculations verified that, at this level of excitation, little or no focusing would be seen. The TRACE calculation, shown in Fig. 38, reveals the action of the RFQ lens on a typical 20-keV proton beam for three different excitations, namely  $B=0$ , 0.3, and 1.2. The difference in the action of the lens for  $B=0$  (off) and  $B=0.3$  (on) is very slight. With the rf-induced electrical noise in the emittance measurement, this small difference would be impossible to

Thu Jun 7 14:55:52 1990

$\epsilon_{rms}$  10.3  $\pi$  mm-mrad  
 $\alpha_{rms}$  -.488  
 $\beta_{rms}$  .252 mm/mrad  
 $\gamma_{rms}$  4.92 mrad/mm  
 KE 0.0336 Mev  
 Toroid 49 mA

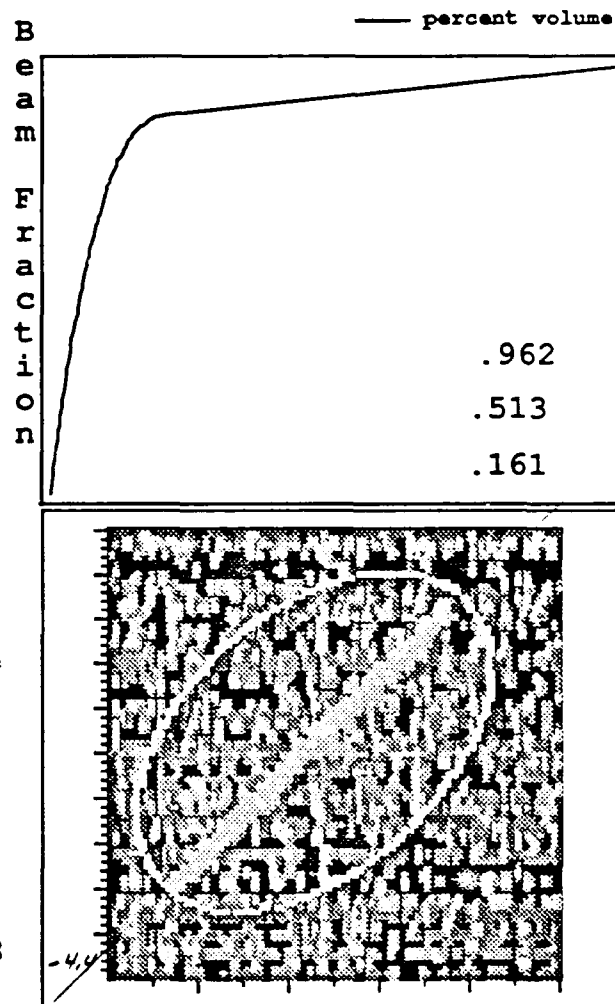
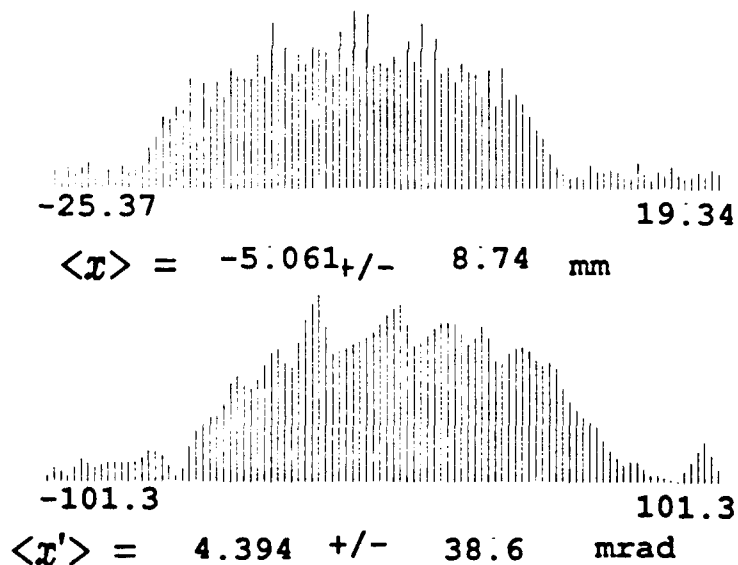


Fig. 36. Emittance Scan of Beam with RFQ Lens Off.

Thu Jun 7 14:58:48 1990

$\epsilon_{rms}$  15.8  $\pi$  mm-mrad  
 $\alpha_{rms}$  -0.002  
 $\beta_{rms}$  .394 mm/mrad  
 $\gamma_{rms}$  2.54 mrad/mm  
 KE 0.0337 Mev  
 Toroid 51.3 mA

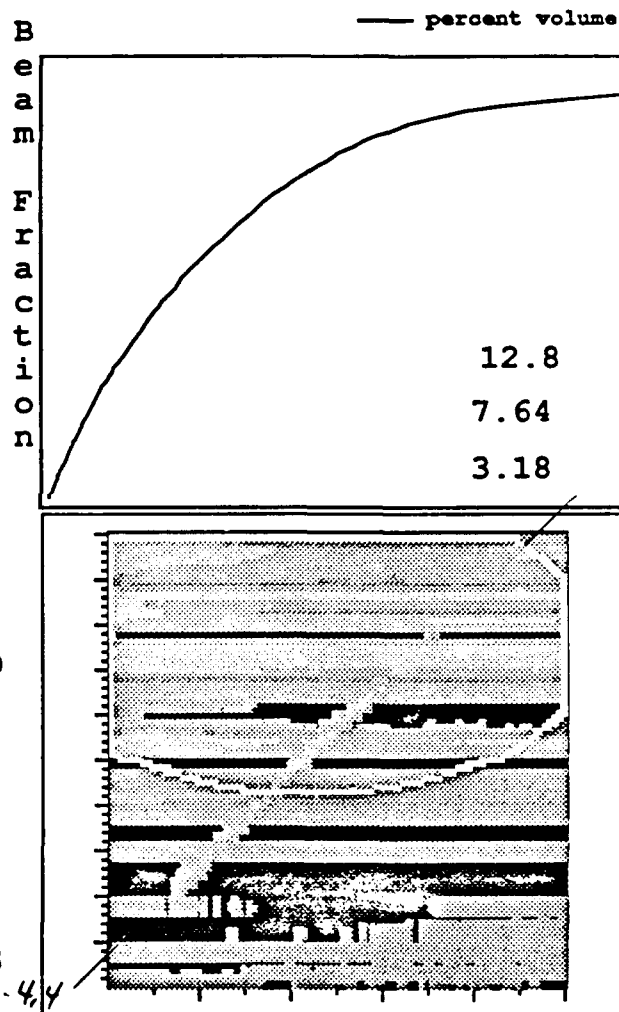
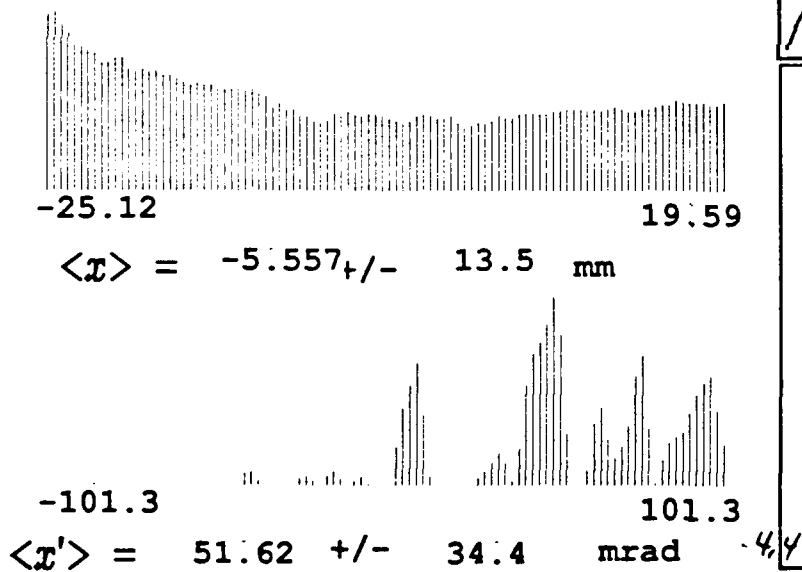


Fig. 37. Emittance Scan of Beam with RFQ Lens On.

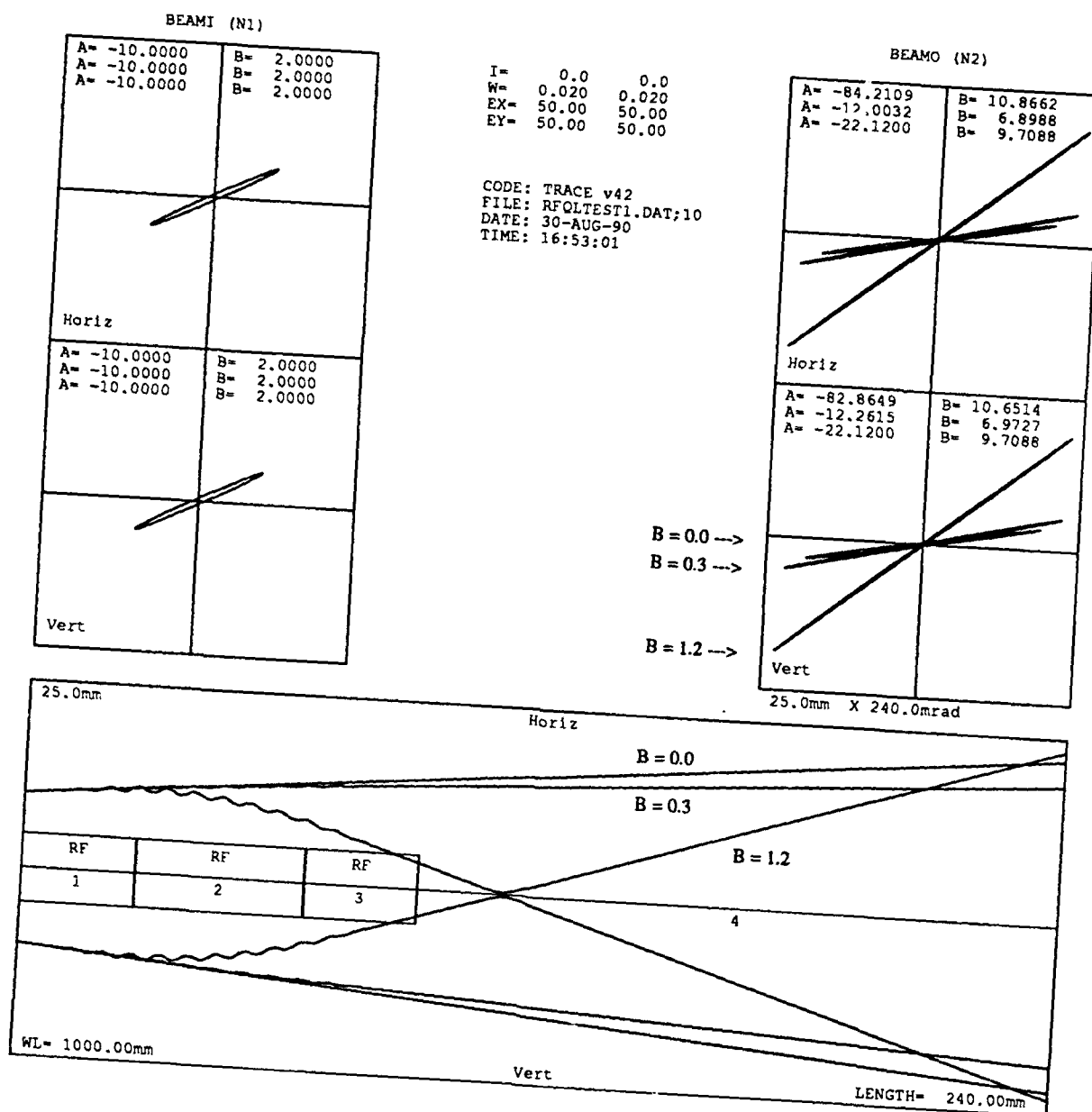


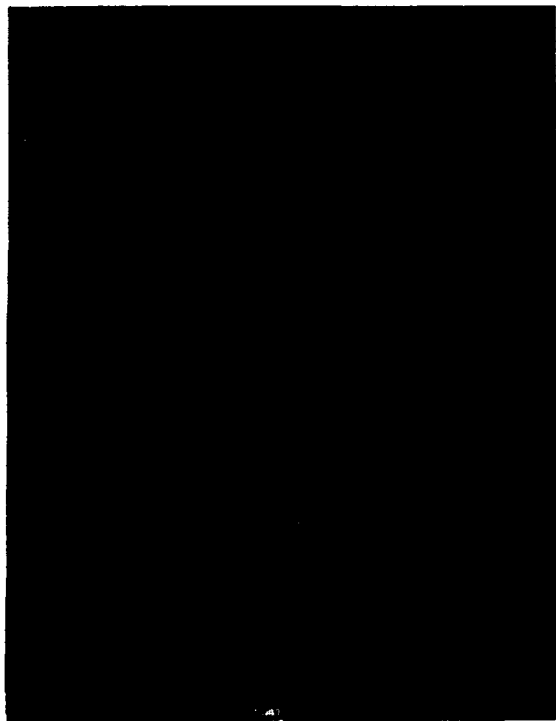
Fig. 38. TRACE for 20-keV Beam and B = 0, 0.3, and 1.2.

observe. The remainder of the fourth day was spent upgrading the rf power system for maximum power output (26 kW), trying to reduce the crosstalk between the rf power system and the emittance scanner, and making additional TRACE calculations.

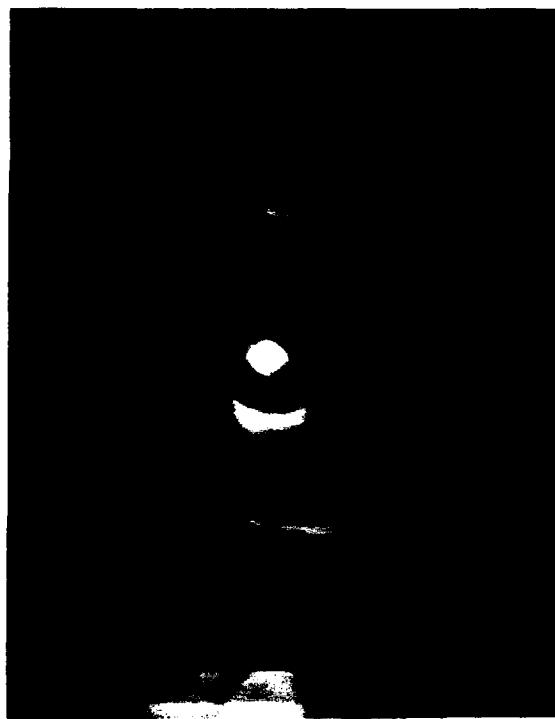
On the fifth day of the experiment a round spot was seen on both the fluorescent viewing screen and the quartz viewing screen. While we do not completely understand this phenomenon, we speculate that the spot is due to the focusing of an undefined component of the ion source beam. This speculation is discussed more fully in Section 9. The round nature of the spot is a valuable feature of the RFQ lens, indicating similar action of the lens on both transverse components of the beam. The radius of the spot responded to changes in lens excitation as expected. A sequence of these spots for different lens excitations, is shown in Fig. 39. The smallest spot (a) corresponds to the case where the beam is focused on the screen with a vane-to-vane voltage of 14.9 kV ( $B=0.16$ ). When the lens excitation is increased (b, c, and d), the spot radius increases as the beam comes to a focus before the screen and then diverges as it expands to the plane of the screen.

As indicated in Section 7, the power of this lens was inadequate to focus the principal component of the beam (20 keV protons) to the observed spot on the viewing screen. Nevertheless, the observation of this phenomenon, assuming it involves the focusing of some undefined component of the beam to a well-defined circular spot on a viewing screen, constitutes a valuable proof-of-principle test of the RFQ lens.





a) Vane-to-Vane Voltage = 14.9 kV.



b) Vane-to-Vane Voltage = 18.7 kV.



c) Vane-to-Vane Voltage = 20.5 kV.



d) Vane-to-Vane Voltage = 28.0 kV.

Fig. 39. Beam Spots Produced During Beam Test of RFQ Lens.

## 9. POST BEAM TEST OBSERVATIONS

An effort was made to find an explanation for the spots that were seen on the last day of the beam experiments at Fermilab. Beam components involving heavier particles, lighter particles, higher charge states, and lower energies were considered. There is some chance that there are some 20-keV molecular oxygen, nitrogen, or water vapor ions in the beam. TRACE indicates, however, that these ions, being 14-to-18 times heavier than protons, would be focused less strongly than protons and do not provide an explanation for the observed spot. Electrons, on the other hand, are so light that the lens excitation was hundreds of times too strong to focus them into a spot. TRACE indicates that the mass of the 20-keV particle that would form a spot, for a lens excitation of  $B=0.16$ , is something like one-twentieth of a proton mass. It is highly unlikely that there are any particles of this mass in the beam. TRACE also indicates that the energy of the proton beam that would form a spot for this lens excitation is 0.28 keV. It is difficult to invent a scenario that could produce protons of this energy in the beam. Due to vacuum conditions, geometric arrangement, and viewing screen response, we conclude that it is unlikely that the spots were formed by x-rays or glow discharge. None of these avenues yield a plausible explanation for the observed beam spot.

As a result of the 3-D ARGUS calculations and pre-beam vane tests, we have a deeper understanding of the interplay of end effects and resonant frequency and vane design. This can be illustrated with a series of SUPERFISH runs. Figure 40 shows a radial section (the two-dimensional SUPERFISH space) through a series of four loaded pillbox cavities. The small geometry on the left, labeled "Base Case", represents the RFQ lens cavity with the original vanes. In this case, it resonates at the relatively high frequency of 559 MHz. In the "Intermediate Case", the frequency has been lowered to 434 MHz by increasing the radius of the tab on the end of the loading post. In the "Loaded Case", corresponding to the RFQ lens cavity as modified, the frequency has been lowered the rest of the way to 300 MHz by reducing the radius of the loading post. Note that, in so doing, both the Q of the cavity has reduced and the power requirement for the cavity has increased by a substantial factor. The large geometry on the right, labeled "Enlarged Case", represents the other viable option for lowering the resonant frequency of the lens, namely to enlarge the diameter of the outer cavity. Note that the Q of the enlarged case is 4.3 times that of the loaded case and that the power requirement of the enlarged case is approximately one-fifth (1/5) that of the loaded case.

Armed with these computational and experimental results, an evolutionary family of RFQ lens geometries emerges and is shown in Fig. 41. The geometry on the left, labeled "Loaded Radial Support", corresponds to the lens that was built and tested during this project. The second

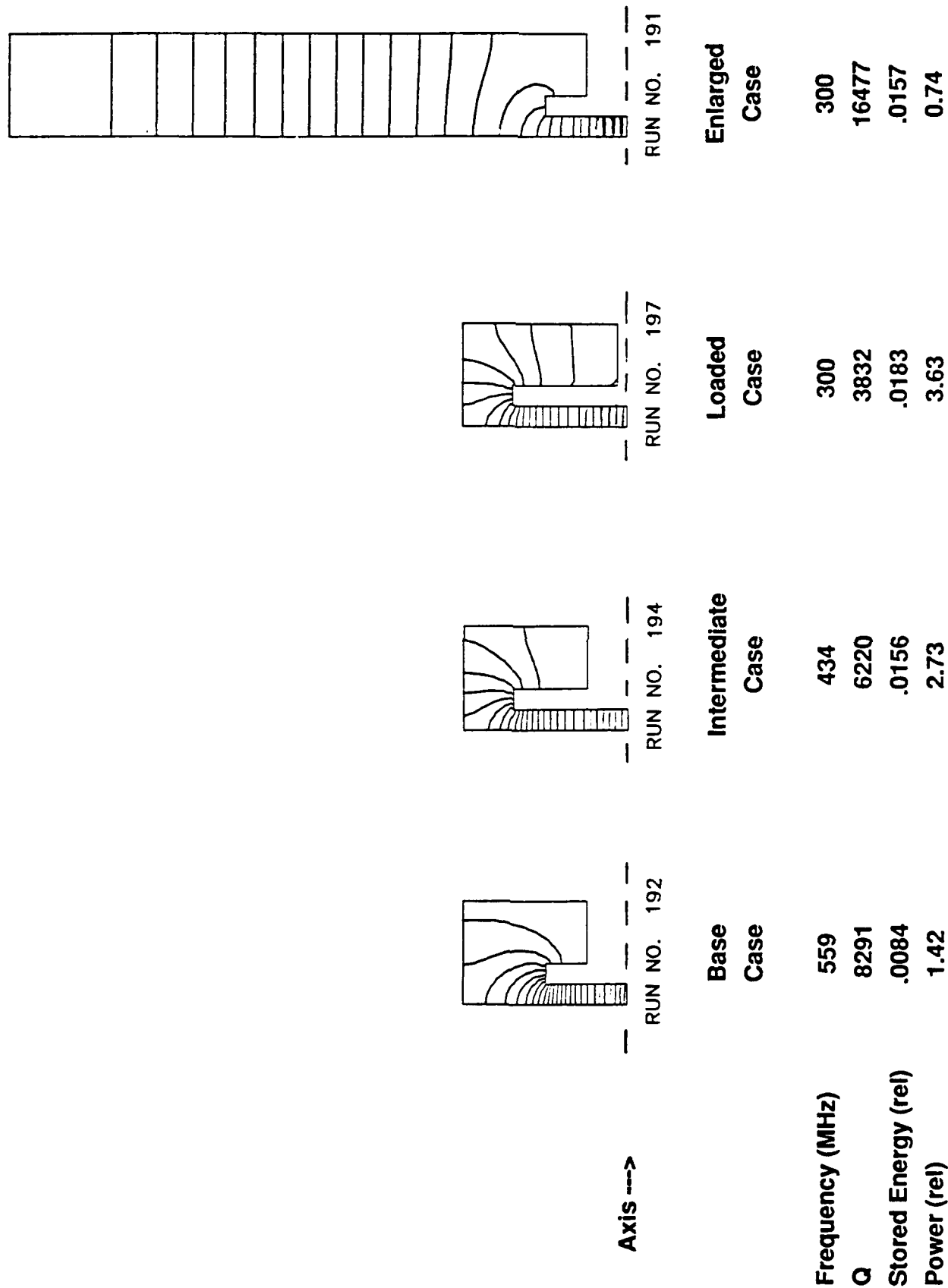


Fig. 40. Cavity Parameters as a Function of Cavity Loading (SUPERFISH).

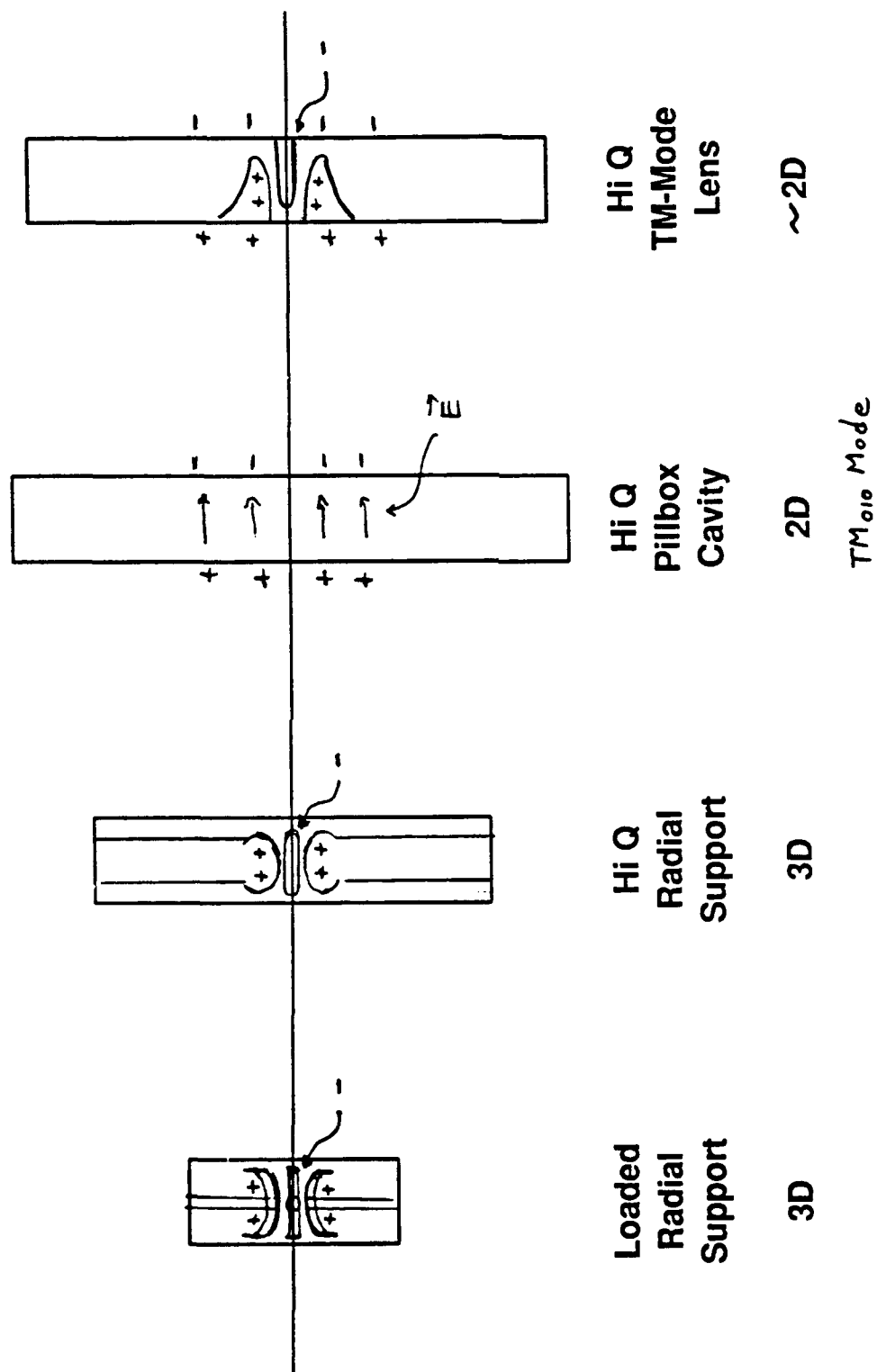


Fig. 41. Family of RFQ Lens Geometries.

geometry from the left corresponds to a larger diameter structure with the original vane geometry, which promises to have a higher Q. The third geometry from the left is not a lens, but suggests the interesting lens geometry shown on the right, namely the high-Q, four-finger, TM-mode, RFQ lens. The four fingers in this geometry present a light capacitive load in the center of a large diameter high Q pillbox cavity. In that respect, it is similar to the enlarged SUPERFISH geometry shown in Fig. 41. SUPERFISH can be used to approximate the electrical performance of this four-finger geometry, which should have a higher rf efficiency than geometries using the radial supports.

Although good design guidance can be obtained from two-dimensional SUPERFISH calculations, the importance of a three-dimensional rf calculational capability is clearly evident from the results reported here. In any future work involving unfamiliar, three-dimensional geometries, we would employ three-dimensional calculations to obtain essential frequency and performance data.

As discussed above, an RFQ lens cavity with 5 times the rf efficiency than the lens constructed here can be built. In combination with an rf power source with 4 times the power available from the present unit an RFQ lens with the desired performance would be within range. As part of the further development of the SAIC accelerator test stand, the Accelerator Technology Division is currently developing a higher-powered CCRF system, based on two higher powered, Eimac YU-176 Planar Triodes. The new unit should be capable of producing 60-80 kW of peak rf power. The test stand produces a proton beam suitable for testing RFQ lenses. This factor of 20 in the (efficiency x power) product offers fields and lens strengths that are larger, by the square root of 20, than those available in the present experiment. This would raise the B-value from the present 0.3 to something in excess of the design value of 1.2.

Another way to increase the B-value of the lens is to lower the rf frequency. By dropping the rf frequency from 300 MHz to 150 MHz, the B-value, which goes inversely as the square of the frequency, would increase from the present value of 0.3 to the design value of 1.2. Due to the requirement for at least  $3\beta\lambda$  matching sections at the entrance and exit to the lens, lower frequency will lengthen the lens and the aperture will have to be increased leading to increased rf power requirements. However, this should be more than offset by the fact that the rf power required (barring length and aperture changes) scales with the inverse of the frequency to the fourth power.

Hence, there appear to be many combinations of higher efficiency, higher power, and lower frequencies that will yield RFQ lenses with useful focal properties.